C.P. No. 577

C.P. No. 577

MINISTRY OF AVIATION

AERONAUTICAL RESEARCH COUNCIL

CURRENT PAPERS

Low-Speed Pressure-Plotting Tests on a Flat-Plate M-Wing Fitted with Part-Span Nose-Flaps

by

L. A. WYATT, Ph.D. and Miss G. P. ILOTT, B.Sc.

LONDON: HER MAJESTY'S STATIONERY OFFICE

1961

SIX SHILLINGS NET

U.D.C. No. 533.693.4 : 533.694.2 : 533.69.048.2

C.P. No. 577
June, 1960

LOW-SPEED PRESSURE-PLOTTING TESTS ON A FLAT-PLATE M-WING FITTED WITH PART-SPAN NOSE-FLAPS

by

L.A. Wyatt, Ph.D.
and
Miss G.P. Ilott, B.Sc.

SUMMARY

Pressure-plotting measurements have been made over the inboard panel of a 55° swept flat-plate M-wing of aspect ratio 5.0 fitted with constant-chord nose-flaps.

The effect of drooped nose-flaps on the pressure distribution over the inboard panel of the M-wing has been found at three overall lift-coefficients of 0.230, 0.514 and 0.718.

Analysis has shown that the loss of stability (pitch-up) which occurs on the M-wing above a lift coefficient of 0.4 can be ascribed to a loss of lift in the neighbourhood of the wing root, and the action of nose-flaps in eliminating this pitch-up has been explained.

Previously issued as R.A.E. Tech. Note No. Aero 2689 - A.R.C.22,504.

LIST OF CONTENTS

LIST OF TABLES

LIST OF ILLUSTRATIONS

LIST OF ILLUSTRATIONS (Contd)

1 INTRODUCTION

In the course of an investigation into wings designed to cruise with attached shock-free flow at low supersonic speeds, Bagley[1] has suggested two suitable planforms, one being an M-wing whose aspect ratio, sweep and section shape are determined by the lift/drag ratio required for the cruise condition. Several such M-wing planforms have been tested, flat-plate models with sharp leading-edges being used to reproduce the leading-edge separations which will be encountered in the low-speed flow over the thin high-speed section at off-design incidences.

Although later work has suggested that a lower aspect ratio is required, earlier emphasis had been placed on a wing of aspect ratio 5.0 with the kink at mid-semi-span. The sweep forward of the quarter-chord line of the straight-tapered inner panel and the sweepback of the trailing edge of the outer panel are both 55°, and the outer panel has a curved leading-edge with a streamwise tip.

Initial tests on this planform showed that the loss of stability (pitch-up) occurring at a lift coefficient of order 0.4 to 0.5 could be cured by drooping nose-flaps on the inner panels, and pressure-plotting measurements were therefore undertaken to determine the aerodynamic mechanism of the nose-flap action. The tests were made in the 13 ft × 9 ft low-speed wind tunnel at R.A.E. Bedford.

2 DETAILS OF MODEL

The model layout is shown in Fig.1, and the model dimensions and the geometry of the wing planform are given in Tables 1 and 2 respectively. The nose-flaps were divided into inner and outer sections of equal span which could be drooped separately or jointly through an angle of 30° perpendicular to the hinge line i.e. 18° 30' in a streamwise direction. The nose-flap chord was constant and equal to 25% of the kink chord. The wing had a symmetrical flat-plate section of constant thickness (0.75 in.) with sharp bevelled leading and trailing edges.

Nine pressure tubes were laid just below both surfaces of one inner panel of the wing along constant percentage chord lines of x/c = 0.20, 0.25, 0.30, 0.35, 0.40, 0.50, 0.60, 0.70 and 0.80, and seven chordwise rows of pressure holes were obtained by drilling into these tubes at spanwise η intervals of 0.0625 (1/16) between η = 0.0625 and 0.4375 (see Fig.1). The pressure tubes were brought out at the rear of the wing on the centre-line. The internal chambers of the hollow nose-flap sections were connected to extra pressure tubes recessed into the wing, so that, by drilling through the nose-flap wall, the pressure could be obtained at any point on the nose-flaps, except close to the leading-edge.

3 DETAILS OF TESTS AND ANALYSIS

Using a conventional wire rig, the model was suspended in the inverted position on the tunnel centre-line. The model was adequately supported to eliminate differential deflections of the inner and outer panels of the wing at a fixed nominal incidence. Previous tests at Bedford on this planform used a smaller scale model which was unduly flexible under load, giving rise to uncertainty in the geometrical incidence. On the model used in the present tests, it made little difference to the nose-flap efficiency in suppressing the pitch-up whether the whole nose-flap span was drooped or only the outer section, whereas, on the smaller model, deflection of the outer section alone had proved distinctly more promising. This slight difference in characteristics was probably due to the improved behaviour of the larger model under load.

The measurements were taken at a wind speed of 150 ft/sec, giving a Reynolds number of 1.8×10^6 based on the aerodynamic mean chord. The overall lift and pitching moment of the clean wing were first measured at nominal incidences of 5°, 10° and 15°, giving lift coefficients $\bar{C}_L$ of 0.230, 0.514 and 0.718 respectively, and the incidences necessary to reproduce these values of $\bar{C}_L$ with the nose-flaps drooped were then determined. Pressure plotting measurements were made at the above $\bar{C}_L$ values on the inner panel of the wing (a) with the nose-flaps neutral, (b) with the outer section of the nose-flaps drooped, and (c) with both nose-flap sections drooped together.

The pressure, force and moment coefficients quoted have not been corrected for the combined effects of solid and wake blockage: the maximum correction would be about -1.0% at $\bar{C}_L = 0.730$. This omission does not affect the final comparison of the overall balance measurements with the lift and pitching moment due to the inner panel computed from the pressure measurements. The analysis of the pressure measurements was made in the usual manner, and the relations used are included in the list of symbols.

4 TYPE OF FLOW

The "titanium dioxide + oil" technique was used to study the flow patterns on the wing surfaces over the whole incidence range 0° to 15°. Due to difficulties with the technique, the photographs of the flow are unsuitable for reproduction, but the salient features of the flows could easily be discerned by eye and are described below. The upper surface flow appropriate to the three configurations at the medium $\bar{C}_L$ of 0.514 is sketched in Fig.2, and, to illustrate the effect of nose-flap droop, sections through the flow near the leading-edge are given in Fig.3.

4.1 Flow pattern on clean wing

The dominating feature of the flow over the clean wing is a full leading-edge separation at all non-zero incidences. On both panels of the M-wing, the separated layers roll up into coiled vortex sheets radiating from the leading-edge apex at mid-semi-span. On the inner panel, the coiled sheet breaks away from the leading-edge in the neighbourhood of the swept forward junction at the wing root, and turns down stream.

The flow patterns on the upper surface of the wing show clearly the region covered by the leading-edge vortex flow, e.g. in Figs.2(a) and 3(a), the region between the primary separation line P at the leading-edge and the attachment line A. The surface flow upstream of A is towards the leading-edge, and shows a secondary separation along the line S. The flow structure between the primary and secondary separation lines on the inner panels was not distinct in the present experiments, due to disturbances caused by small discontinuities along the leading-edge at the nose-flap junctions and by the bevel line on the nose-flaps. At $\alpha = 10°$, approximately half the area of the inner panel is covered by the leading-edge vortex flow. Even at 5° incidence, there is a detectable inflow at the trailing-edge of the air which has come over the rolled-up vortex sheet, and, at $\alpha = 15°$, the flow at the trailing-edge is parallel to the trailing-edge over nearly all its length. At $\alpha = 15°$, the flow at the wing root is beginning to break down with the formation of reversed flow (and possibly a bubble) near the leading-edge. At the higher incidences, the vortex which is turning downstream at the wing root is unable to penetrate as close to the root.

The leading-edge sweep of the inner panel of the M-wing is 50.6° and this seems to be rather marginal for the ready development of the coiled vortex sheet at the lowest incidences below 5°. The definition of the vortex at small incidences is much better on wings of higher sweep, e.g. on the various members of a series of slender wings described by Peckham[2], and the definition is slightly better even on the outer panel of the present M-wing, where the initial leading-edge sweep is 55°.

4.2 Effect of nose-flap droop

The flow patterns due to drooping the outer section and the whole length of the nose-flaps at $\bar{C}_L = 0.514$ are shown in Figs.2(b), (c). With the outer section only drooped, the flow pattern develops as follows. There is attached flow over the upper surface of the drooped nose-flap section, its direction being nearly normal to the leading-edge. At $\alpha = 0°$ and 5°, there is a small bubble on the nose-flap hinge marked by an accumulation of oil which slowly drains along the hinge line and is swept away over the upper surface by a small streamwise edge vortex springing from the leading-edge discontinuity (effectively a notch) at $\eta = 0.25$. A similar edge vortex originates at mid-semi-span. The flow over the inner section of the inner panel is dominated by a leading-edge vortex turning downstream at the root. At an incidence between 5° and 10°, the hinge line bubble is replaced by a separation leading to a coiled vortex sheet which will be considerably weaker than that springing from the leading-edge of the inner section of the panel at the same incidence. This new vortex sheet turns downstream at approximately $\eta = 0.25$. It is interesting to note that the vortex from the hinge line does not appear to have any associated secondary separation, presumably because of its lower strength. At an incidence of 15°, flow breakdown in the shape of reversed flow is occurring not only at the root but also near the nose-flap hinge at $\eta = 0.25$. The flow near the trailing-edge is further from the free-stream direction than on the clean wing; this confirms the observed detrimental effect of drooping the outer nose-flaps on the efficiency of plain trailing-edge flaps.

If both outer and inner nose-flap sections are drooped together, the flow at low incidences is again marked by a bubble on the nose-flap hinge line, which is replaced by a weak coiled vortex sheet between $\alpha = 5°$ and 10°. The area of the wing covered by the vortex flow increases with incidence, but is displaced downstream relative to that on the clean wing because its origin is at the hinge line rather than at the leading-edge. At higher incidences, the attached flow over the drooped nose-flap helps to reduce the extent of the flow breakdown at the root.

The surface flow was visualized with the inner flap alone deflected but time was not available for pressure plotting this configuration. With the inner nose-flap drooped, the leading-edge vortex from the outer section of the panel is accompanied by a weaker vortex from the nose-flap hinge line at the higher incidences, and the wing area covered by the vortex flows is roughly equal to that covered by the flow field of the single leading-edge vortex on the clean wing. Drooping the inner nose-flap section does not remove the pitch-up of the wing, but it does help the efficiency of plain trailing-edge flaps, and tuft tests at R.A.E., Farnborough, have confirmed that the flow in the wing root is improved.

On the lower surface, outflow develops near the trailing-edge. In conjunction with the marked inflow occurring on the upper surface, this corresponds to vorticity being shed from the trailing-edge which is opposite in sign to that of the leading-edge vortex from the same panel. Kirby[3] has described the complete trailing vortex system more extensively in a note discussing the same M-wing planform in combination with a body.

The above description of the flow patterns will be related to the pressure distributions measured on the wing.

5 CHORDWISE PRESSURE AND LOAD DISTRIBUTIONS

This section gives typical examples of the effect of nose-flap droop on the surface pressure and load distributions on the inner panel of the M-wing. Overall lift and pitching moment characteristics of the wing are shown in Fig.4. To demonstrate the effect of nose-flap droop, we use the pressure and load distributions measured at the medium $\bar{C}_L$ of 0.514 at $\eta = 0.25$ on (a) the clean wing, and (b) the wing with all nose-flaps drooped (see Fig.5). The $\eta = 0.25$ position is chosen as being furthest from the "centre" effects of the junctions at the root and mid-semi-span. Fig.6 shows how the load distribution varies with $\bar{C}_L$ in the two cases.

5.1 Effect of nose-flap droop; $\eta = 0.25$, $\bar{C}_L = 0.514$

On the clean wing, the upper surface pressure distribution (lower half of Fig.5) shows a suction peak at $x/c = 0.2$ due to the coiled leading-edge vortex. A tendency to form a secondary peak around $x/c = 0.08$ may be ascribed to the flow between the secondary separation line and the leading-edge. In the particular example chosen, a positive C_p was registered on the upper surface at $x/c = 0.5$, obviously connected with the attachment. Study of the relevant oil flow photograph suggested that the attachment line lay at x/c of order 0.4, and that the positive peak was registered at the point downstream of which the flow direction is roughly constant back to the trailing edge. As found by Peckham in pressure-plotting tests on sharp edged delta and gothic wings[2], the main suction peak occurs at the "downstream" end (i.e. nearer leading edge) of the straight section of the flow between the attachment and secondary separation lines.

The load distribution ΔC_p on the clean wing (see Fig.6) is very similar to the upper surface pressure distribution with a maximum at 20% chord. Aft of this point, the load decreases rapidly and, until the incidence exceeds 10°, only about 5% of the total load is developed over the rear half of the section. Reference to Fig.25 shows that the centre of pressure, x_{CP}, is at 20% chord.

At the same $\bar{C}_L$ of 0.514, nose-flap droop radically changes the pressure and load distributions. The main suction peak is now due to the attached flow on the upper surface of the nose-flaps, and occurs at $x/c = 0.08$ or a little further forward. A secondary peak around $x/c = 0.2$ is due to the weaker coiled vortex springing from the nose-flap hinge line. The pressure recovery towards the trailing-edge is fairly uniform in this case.

The two peaks in the load distribution are less marked because of the effect of the leading-edge separation on the lower surface. The load is concentrated more to the rear of the section, and falls almost linearly from $x/c = 0.3$ to the trailing edge. Just over 25% of the total load occurs on the rear half of the section, and the centre of pressure position is now $x_{CP}/c = 0.3$ i.e. 10% of the chord behind the clean wing position.

Hence, well away from the junctions of the M-wing, the effect of drooping the nose-flaps at constant $\bar{C}_L$ is to shift the local centre of pressure rearwards by a substantial amount, which will give a negative pitching moment increment. At the same time, the sectional C_L is decreased by the droop -

see Fig.16. The effect of this lift loss on the pitching moment depends on the position of the centre of pressure relative to the mean quarter-chord line.

5.2 Variation with lift coefficient; $\eta = 0.25$

The variation in the chordwise load distribution with $\bar{C}_L$ at $\eta = 0.25$ is shown in Fig.6, with and without all nose-flaps drooped. As the leading-edge vortex grows on the clean wing, the main suction peak moves rearwards. A large movement occurs between $\bar{C}_L = 0.230$ and 0.514 from $x/c = 0.05$ to 0.20, but the next increase of $\bar{C}_L$ to 0.718 only moves the peak back to 0.25. At the highest $\bar{C}_L$, the secondary peak at $x/c = 0.06$ is well marked. The corresponding centre of pressure positions are 22, 20 and 28% of the chord i.e. there is little change up to $\bar{C}_L = 0.5$ followed by a rearward shift: this is connected with the turning downstream of the vortex flow at the wing root, which results in the build up of load over the rear part of the chord.

If all the nose-flaps are drooped, the suction peak due to the attached flow moves forward with increasing $\bar{C}_L$, reaching $x/c = 0.04$ at $\bar{C}_L = 0.718$. At the lowest $\bar{C}_L$, the peak is back at 20% chord, because the strong leading-edge separation below the wing reduces the load forward of that point, negative load being recorded near the leading-edge. At all $\bar{C}_L$ values, the load decreases steadily from x/c of order 0.3 or 0.4 to the trailing-edge. The secondary peaks at $x/c = 0.2$ are due to the vortex separating from the hinge line. The respective centre of pressure positions are $x_{CP}/c = 0.32$, 0.31, 0.28 i.e. a small but steady forward shift with increasing incidence.

When only the outer section of the nose-flaps is drooped, the flow inboard of the centre of the inner panel will be of the clean wing type, and that outboard will be of the drooped nose-flap type.

5.3 Isobars and loadings on inner panel

To supplement the discussion of sections 5.1 and 5.2, detailed isobar plots and load distributions over the inner panel are provided in Figs.7 to 15 for the three wing configurations at the three lift coefficients $\bar{C}_L = 0.230$, 0.514 and 0.718. The load distributions are drawn to scale, though the scale is not constant for all the figures. With the outer section of the nose-flaps deflected, there is a discontinuity in the load distribution at $\eta = 0.25$ forward of the nose-flap hinge; in this case, the dotted curve refers to the wing immediately inboard of $\eta = 0.25$ and the full curve to the region immediately outboard. The isobar plots are supplemented by the addition of peak suction lines, no distinction being made as to whether they are due to attached or separated vortex flow. No ambiguity should arise if the isobars and load distributions are consulted in conjunction with the flow descriptions of section 4.

The main features displayed by the isobars and load distributions will now be outlined. Fig.7 refers to the clean wing at $\bar{C}_L = 0.230$. The upper surface peak suction line lies almost parallel to the leading-edge, and does not radiate from the leading-edge apex as it would if due to a well-defined leading-edge vortex - this behaviour is undoubtedly due to the irregularities in the leading-edge splitting the leading-edge separation and delaying its development. Similar behaviour is shown between $\eta = 0$ and 0.25 in Fig.8, which concerns the wing with outer nose-flaps drooped at $\bar{C}_L = 0.230$. Moreover, the peak suctions tend to increase away from the leading-edge apex,

which is not characteristic of a coiled vortex flow. Over the outer drooped section (Fig.8), the upper surface pressures indicate a suction peak along the hinge line. The load distribution shows another peak further forward, which is accentuated by the rapid fall in the load near the leading-edge due to the leading-edge vortex on the lower surface. With all nose-flaps drooped at $\bar{C}_L = 0.230$ (Fig.9), peak suctions are again apparent near the hinge line.

Fig.10 for the clean wing at $\bar{C}_L = 0.514$ shows a well developed leading-edge vortex flow with the peak suction line radiating from the leading-edge apex until the vortex is turned downstream near the root. Moving inwards from mid-semi-span, the initial single peak is gradually superseded by two, the forward one being due to the flow between the secondary separation and the leading-edge. The magnitude of the peak suction falls off rapidly from a maximum of order -3.0 measured at $\eta = 0.438$. A similar maximum can be seen on the inner section of the wing in Fig.11 which covers the case of outer nose-flaps drooped at $\bar{C}_L = 0.514$. The isobars outboard of $\eta = 0.25$ show two suction peaks, one on the hinge line and the other (much sharper) due to the attached flow over the drooped section. This behaviour is reproduced when the whole length of the nose-flaps is deflected at the same $\bar{C}_L$, see Fig.12. The attached flow suction peaks tend to increase towards the wing root. In Fig.12, the peak suction line associated with the vortex from the hinge line is well defined. The load distribution near the leading-edge does not contain any appreciable positive ΔC_p values, indicating the decrease in strength of the lower surface vortex.

The general nature of the results for $\bar{C}_L = 0.718$ is very similar to those for the medium $\bar{C}_L$. On the clean wing (Fig.13), the peak suction line has swung backwards and higher peaks are registered, the largest $C_{P_{US}}$ being of order -5.5. The fall off towards the root is extremely rapid, and this coincides with a broadening of the suction peak. The secondary peak is not so well marked as at $\bar{C}_L = 0.514$. With the outer nose-flaps drooped (Fig.14), the attached flow peak has moved closer to the leading-edge, with a maximum peak suction of order -2.5 being recorded at $\eta = 0.25$. The peak due to the hinge line vortex is more marked than when all the nose-flaps are deflected, as in Fig.15.

6 SPANWISE DISTRIBUTION OF LIFT COEFFICIENT

The spanwise C_L distribution over the inner panel of the three configurations is shown in Fig.16. On the clean wing, the C_L distribution is approximately uniform outboard of $\eta = 0.25$. Inboard of this point, a slight maximum occurs followed by a rapid loss of local C_L at the root. At the three $\bar{C}_L$ values used, the maximum C_L occurs at $\eta = 0.125$, 0.175 and 0.30 respectively, and these positions coincide approximately with the points where the attachment lines bend downstream and become less distinct. The local lift curve slope is roughly constant for $0.25 < \eta < 0.5$, but it falls off increasingly as the root is approached. Sections inboard of $\eta = 0.08$ actually suffer a loss of lift between the $\bar{C}_L$ values of 0.514 and 0.718. This lift loss is consistent with the physical inability of the growing leading-edge vortex to penetrate as close to the wing root at the higher incidences.

When the outer section of the nose-flaps is drooped, the leading-edge separation is confined to the inner section of the panel, and the smaller size of the vortex means that it can penetrate closer to the wing root before turning downstream. At $\bar{C}_L$ = 0.514 and 0.718, this is reflected in the increased C_L measured for η less than 0.15 and 0.23 respectively. The lift on the outer section is reduced due to the loss of the non-linear lift increment from the leading-edge vortex, though this loss is partly replaced at the highest $\bar{C}_L$ by non-linear lift from the weaker vortex springing from the hinge line - this replacement probably accounts for the disappearance of the discontinuity in C_L at η = 0.25. At the root, the local C_L stays approximately constant as $\bar{C}_L$ increases from 0.5 to 0.7.

When all the nose-flaps are deflected, the C_L is reduced for all values of η at $\bar{C}_L$ = 0.230 and 0.514, and is fairly uniform over the semi-span. However, at the highest $\bar{C}_L$ = 0.718, a maximum local C_L is indicated at η = 0.13 (presumably due to the bending downstream of the hinge-line vortex), together with a reduction towards the root. However, at the root, the presence of some attached flow over the nose-flap means that the lift does increase steadily through the incidence range up to 15°.

7 SPANWISE LOAD DISTRIBUTION

Spanwise load distributions for $\bar{C}_L$ = 0.230, 0.514 and 0.718 are shown in Figs.17, 18 and 19. Integration of $cC_L/\bar{c}$ from η = 0 to 0.5 gives the contribution of the inner panel to the overall lift i.e. $\bar{C}_{L_{INNER}}$. The proportion of the load carried by the inner panel remains constant through the incidence range at about 64% for the clean wing and for the wing with the outer nose-flaps drooped, falling to 60% with all nose-flaps drooped. The application of the outer nose-flaps does not lead to a change in the lift carried because the loss of lift over the outer section is counter-balanced by the gain near the root. With all nose-flaps deflected, there is a net loss of lift on the inner panel. The inner panel includes 66.5% of the total wing area, so that the distribution of load on the inner and outer panels of the M-wing is closely proportional to the area distribution. This implies that the lift loss near the root is probably balanced by some loss of lift near the tip of the outer panel.

The loadings at the lowest $\bar{C}_L$ of 0.230 (Fig.17) are compared with a theoretical spanwise loading calculated by Brebner's method[4] for a thin wing with fully attached flow i.e. the limiting loading as C_L tends to zero. Outside the root area, there is close correspondence between the experimental loading on the inner panel and the theoretical values.

8 PITCHING MOMENT CHARACTERISTICS

The pitching moment characteristics of the wing are presented in Figs.20 to 26, which should be consulted together. In Fig.20 for the clean wing, the spanwise variation of $cC_m/\bar{c}\,\bar{C}_m$ is given to illustrate the usual difficulty experienced on integrating the sectional pitching moments on swept wings i.e. that the sectional moments are large compared with the integrated moment about the mean quarter chord point. Figs.21 to 23 show the sectional moments at the three test $\bar{C}_L$ values, and Fig.24 gives the contribution to the overall moment from the inner and outer panels. In Figs.25 and 26, the centre

of pressure position is presented (a) as a fraction of the local chord, and (b) divided by $\bar{c}$ i.e. effectively distance from the local leading-edge.

8.1 Pitching moment of clean wing

The weighted sectional moments C_m for the clean wing are presented in Fig.20. By reference to Fig.24, it may be seen that the contribution of the inner panel to the overall $\bar{C}_m$ is approximately constant at the lower $\bar{C}_L$ values of 0.230 and 0.514, $\bar{C}_{m_{INNER}}$ being about 0.010. However, as $\bar{C}_L$ increases to 0.718, $C_{m_{INNER}}$ rises to 0.044, and this rapid change is the direct cause of the pitch-up manifested in the $\bar{C}_m$, $\bar{C}_L$ curve. The lower figure of Fig.24 shows that the outer panel pitching moment is required to vary almost linearly with $\bar{C}_L$.

The associated changes in centre of pressure position and sectional lift coefficient are given in Figs.25, 26 and 16. Near the leading-edge apex, $0.35 < \eta < 0.5$, the centre of pressure of the clean wing stays close to $x/c = 0.23$ throughout the range of incidence. At $\bar{C}_L = 0.514$ and 0.718, the growth of the leading-edge vortex is reflected in a rearward movement of the centre of pressure for $0.13 < \eta < 0.35$. Between $\bar{C}_L = 0.514$ and 0.718, the rearward movement is replaced by a forward movement for $\eta < 0.13$, due to the growing vortex being forced outboard from the root. This forward movement, when combined with the loss of sectional lift at the root (see Fig.16), is the origin of the pitch-up on the clean wing for $\bar{C}_L > 0.5$. The net effect is shown strikingly in Figs.20 and 23, where the sectional pitching moment on the clean wing at $\bar{C}_L = 0.718$ shows a marked upward sweep for $\eta < 0.13$, corresponding to a loss of stability.

The gradual increase in stability of the clean wing for $\bar{C}_L < 0.3$ (Fig.4) is due to the rearward shift of the centre of pressure as the leading-edge vortex is established - a similar tendency has been observed on a sharp edged gothic wing at low $\bar{C}_L$ values[5]. On the M-wing, however, this stable trend is soon swamped by the pitch-up due to the decrease in lift at the root.

8.2 Effect of nose-flap droop

Figs.21 to 23 show the effect of nose-flap droop on the sectional pitching moments. At the two lowest $\bar{C}_L$ values, the effect of deflecting the outer nose-flaps is to give negative pitching moment increments for $\eta > 0.25$ and $\eta < 0.1$ (Figs.21 and 22). Outboard of $\eta = 0.25$, the nose-down pitch is due to a loss of non-linear lift combined with a substantial rearward movement of the centre of pressure of about 10% local chord. At the root, the smaller leading-edge vortex penetrates closer to the centre-line giving some extra lift behind the pitching moment axis: this negative increment is however much smaller than that generated on the outer drooped section. At the highest $\bar{C}_L = 0.718$, the favourable increment from the root section becomes more nearly equal to that from the outer section, and a helpful rearward movement of the centre of pressure at the root occurs as the leading-edge vortex expands. Fig.24 shows that the inner panel with the outer nose-flaps drooped still shows some pitch-up for $\bar{C}_L > 0.5$, but the change of slope is smoothed out somewhat in the overall $\bar{C}_m$ curves.

At $\bar{C}_L = 0.230$, drooping all the nose-flaps gives a negative pitch increment over the whole half semi-span (Fig.21), due again over the outer section to a loss of non-linear lift combined with a rearward centre of pressure movement. Over the inner section, little lift loss is found and the increase of x_{CP} is the main factor. At the root, deflection of all the nose-flaps at $\bar{C}_L = 0.718$ gives almost twice the nose-down increment found with only the outer section deflected. This corresponds to the marked lift increase at the root visible in Fig.16. The integrated value of $\bar{C}_{m_{INNER}}$ shows a negligible loss of stability at $\bar{C}_L$ greater than 0.5, and this is reflected in the $\bar{C}_m$ values.

9 COMMENT ON RESULTS

Previous sections have described how pressure plotting measurements on the inner panel of an M-wing have accounted for the pitch-up experienced at moderate $\bar{C}_L$ in terms of a loss of lift at the root. The operation of nose-flap droop in reducing the pitch-up has been explained. On the clean wing, the pitch-up computed on the inner panel is, if anything, more than enough to account for the overall measured pitch-up.

The outer panel pitching moment must apparently vary linearly with $\bar{C}_L$. This conclusion is somewhat surprising. Kirby and Johnson's results[3] and some American tests[6] indicate that the outer panel of the M-wing (which is equivalent to half a swept wing of aspect ratio 3.75) should show some pitch-up around a $\bar{C}_L$ of 0.5. A likely value for the loss in stability would seem to be a change in $d\bar{C}_m/d\bar{C}_L$ of order 0.25. Adaption of this result to the case of the M-wing, by allowing for the changes in reference area and aerodynamic mean chord, suggests that the outer panel ought to contribute 0.04 to the change in $d\bar{C}_m/d\bar{C}_L$ on the complete M-wing. The actual change on the M-wing is of order 0.15, all of which can be ascribed to the inner panel, and, although the pressure plotting results did not actually cover $\eta = 0$ and $\eta = 0.5$, it is not considered that the mode of extension of the existing results to these limits (e.g. in Fig.23) could affect the integrated moments sufficiently to account for any such discrepancy. On the M-wing, the outer panel is in the downwash field of the adjacent inner panels, and it is just possible that any tendency to pitch-up of the outer panel is balanced by suitable downwash variations. In any case, the outer panel would be unlikely to contribute more than 25% of the measured pitch-up.

It is of interest to note that the pitch-up still occurs in the presence of a body[3], although it is somewhat masked by the large unstable moment derived from the body, and that the nose-flaps are still effective in reducing the pitch-up.

10 CONCLUSIONS

The inner panel of an M-wing with sharp leading-edges has been extensively pressure plotted to discover why drooped nose-flaps are effective in reducing the pitch-up which occurs above a $\bar{C}_L$ of 0.4 to 0.5 on the clean wing.

The pitch-up may be explained in terms of a loss of lift occurring near the wing root at higher $\bar{C}_L$ values, when the leading-edge vortex growth is such that it cannot penetrate as close to the centre line. This lift loss constitutes a loss of stability about the mean quarter chord point.

If the outer section of the nose-flaps is drooped, the pitch-up is alleviated. The improvement is largely accounted for by a loss of lift over the outer section of the inner panel, combined with a large rearward travel of the centre of pressure, due to the replacement of the leading-edge vortex by attached flow over the nose-flap, with a weaker vortex from the nose-flaps hinge developing at higher incidences. The nose-flap action is also helped by an increase of lift at the wing root due to the closer approach to the centre line of the smaller leading edge vortex off the undisturbed inner leading-edge.

An equally beneficial effect on the pitch-up is achieved by drooping nose-flaps over the whole of the inner panel. The outer section of the panel again contributes a nose-down pitch due to the rearward movement of the centre of pressure and due to the loss of lift, which is favourable as it is concentrated ahead of the mean quarter chord. An equal effect is contributed at higher $\bar{C}_L$ by increased lift near the wing root which is concentrated nearer the trailing-edge.

LIST OF SYMBOLS

A	aspect ratio
b	wing span
S	wing area
c	local chord
$\bar{c}$	$= S/b$, geometric mean chord
$\bar{\bar{c}}$	$= \int_0^1 c^2 \, d\eta \Big/ \int_0^1 c \, d\eta$, aerodynamic mean chord
x	streamwise distance from wing leading-edge
y	spanwise distance from wing root
η	$= 2y/b$, non-dimensional spanwise co-ordinate
$\ell_{\frac{1}{4}}$	distance of mean quarter chord point from T.E. vertex of M-wing
$x_{\frac{1}{4}}$	distance of mean quarter chord point behind local leading-edge
α	incidence
$\bar{C}_L$	overall lift coefficient
$\bar{C}_m$	overall pitching moment coefficient about the mean quarter chord point, based on aerodynamic mean chord

LIST OF SYMBOLS (Contd)

$C_{P_{US}}$, $C_{P_{LS}}$ — upper and lower surface pressure coefficients

$\Delta C_P = C_{P_{US}} - C_{P_{LS}}$, local load

$C_N = -\int_0^1 \Delta C_P \, d\left(\frac{x}{c}\right)$, sectional normal force coefficient

$C_L = C_N \cos \alpha$, sectional lift coefficient

$C_{m_{LE}} = \int_0^1 \Delta C_P \frac{x}{c} \, d\left(\frac{x}{c}\right)$, sectional pitching moment coefficient about leading edge

$x_{CP} = -C_{m_{LE}}/C_N$, distance of local centre of pressure behind leading-edge

$\bar{C}_{L_{INNER}} = \int_0^{0.5} \frac{c}{\bar{c}} C_L \, d\eta$, contribution of inner panel to overall lift coefficient

$C_m = \frac{c}{\bar{c}}\left(C_{m_{LE}} + C_N \frac{x_{\frac{1}{4}}}{c}\right)$ sectional pitching moment coefficient about the mean quarter chord point, based on the aerodynamic mean chord

$\bar{C}_{m_{INNER}} = \int_0^{0.5} \frac{c}{\bar{c}} C_m \, d\eta$, contribution of inner panel to overall pitching moment coefficient

$\bar{C}_{m_{OUTER}} = \bar{C}_m - \bar{C}_{m_{INNER}}$, contribution of outer panel to overall pitching moment coefficient

$\Delta\bar{C}_m$, $\Delta\bar{C}_{m_{INNER}}$, $\Delta\bar{C}_{m_{OUTER}}$ — pitching moment coefficient increments, relative to clean wing

---

LIST OF REFERENCES

No.	Author(s)	Title, etc.
1	Bagley, J.	An aerodynamic outline of a transonic transport aeroplane. A.R.C. 19,205, October, 1956.
2	Peckham, D.H.	Low-speed wind-tunnel tests on a series of uncambered slender pointed wings with sharp edges. A.R.C. R & M 3186, December, 1958.
3	Kirby, D.A., Johnson, E.M.	Low-speed wind-tunnel tests on 55° sweptback and M-wing models with conventional tail units. Unpublished M.O.A. Report.
4	Brebner, G.G.	The calculation of the loading and pressure distribution on cranked wings. A.R.C. R & M 2947, January, 1953.
5	Peckham, D.H., Atkinson, S.A.	Preliminary results of low speed wind tunnel tests on a gothic wing of aspect ratio 1.0. A.R.C. C.P. 508, April, 1957.
6	Wetzel, B.E.	Effect of taper ratio on lift, drag and pitching moment characteristics of thin wings of aspect ratio 3 with 53.1° sweepback of leading-edge at subsonic and supersonic speeds. NACA/TIB/4535. January, 1955.

TABLE 1

Dimensions of M-wing model

Aspect ratio, A	5.02
Model span, b	8.333 ft (100 in.)
Gross model area, S	13.84 sq ft
Aerodynamic mean chord, $\bar{\bar{c}}$	1.938 ft
Geometric mean chord, $\bar{c}$	1.660 ft
Distance of mean $\frac{1}{4}$ - chord point ahead of T.E. vertex, $\ell_{\frac{1}{4}}$	3.689 ft

TABLE 2

Geometry of M-wing planform

Distribution of local chord c over the semi-span b/2 is given by

$$\frac{c}{b/2} = 0.74 - 0.84\,\eta \quad , \quad 0 < \eta < 0.5$$

$$\frac{c}{b/2} = 0.64\left[\sqrt{2(1-\eta)} - (1-\eta)\right], \quad 0.5 < \eta < 1.0$$

Wing area, $S = 0.7967\ (b/2)^2$

Aerodynamic mean chord, $\bar{\bar{c}} = 0.4652\ (b/2)$

Geometric mean chord, $\bar{c} = 0.3983\ (b/2)$

Distance of mean $\frac{1}{4}$ - chord point ahead of T.E. vertex, $\ell_{\frac{1}{4}} = 0.8853\ (b/2)$

WT.2078.C.P.577.K3 - Printed in England

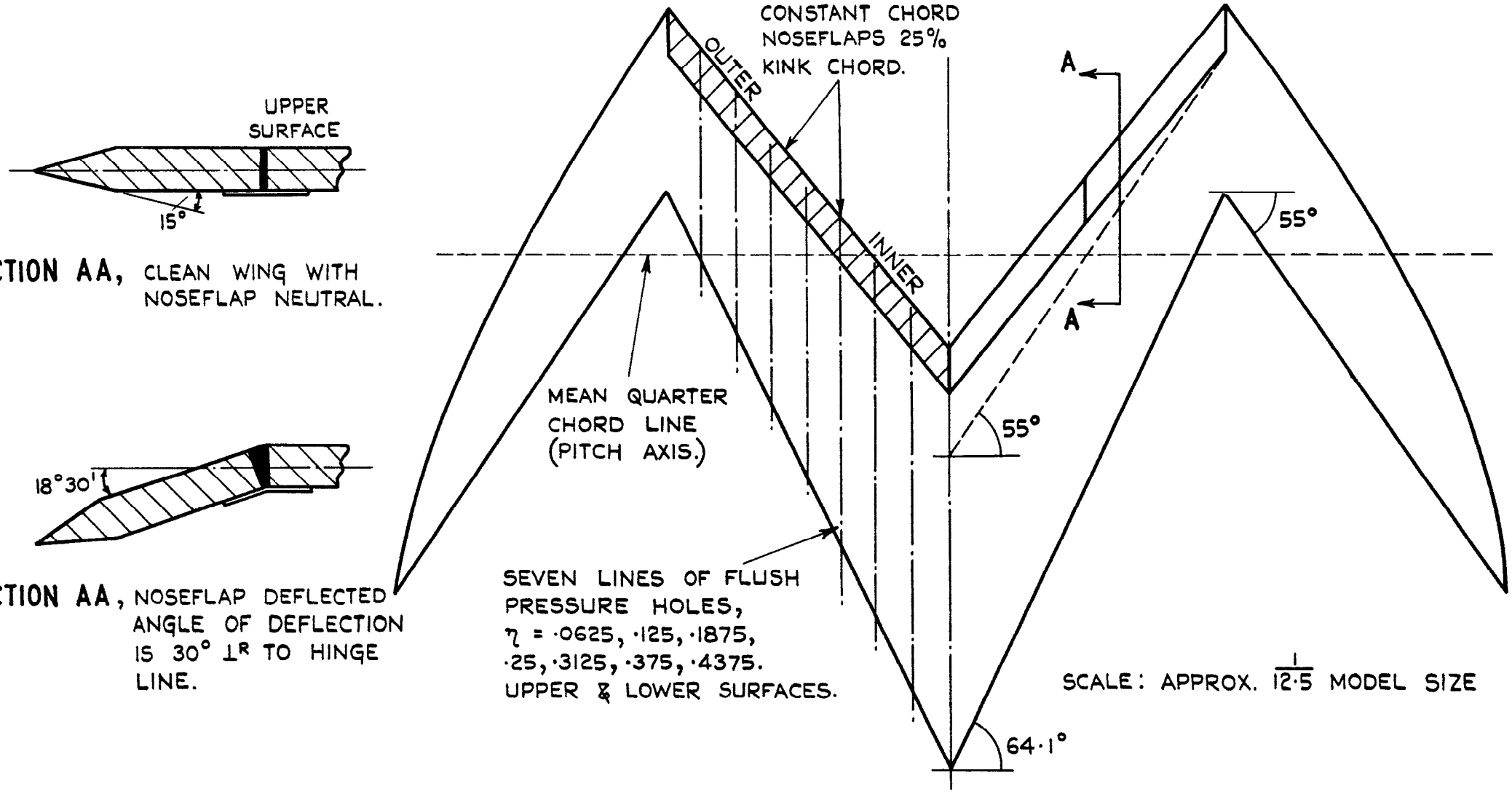

FIG. 1. GENERAL ARRANGEMENT OF MODEL WITH NOSEFLAPS.

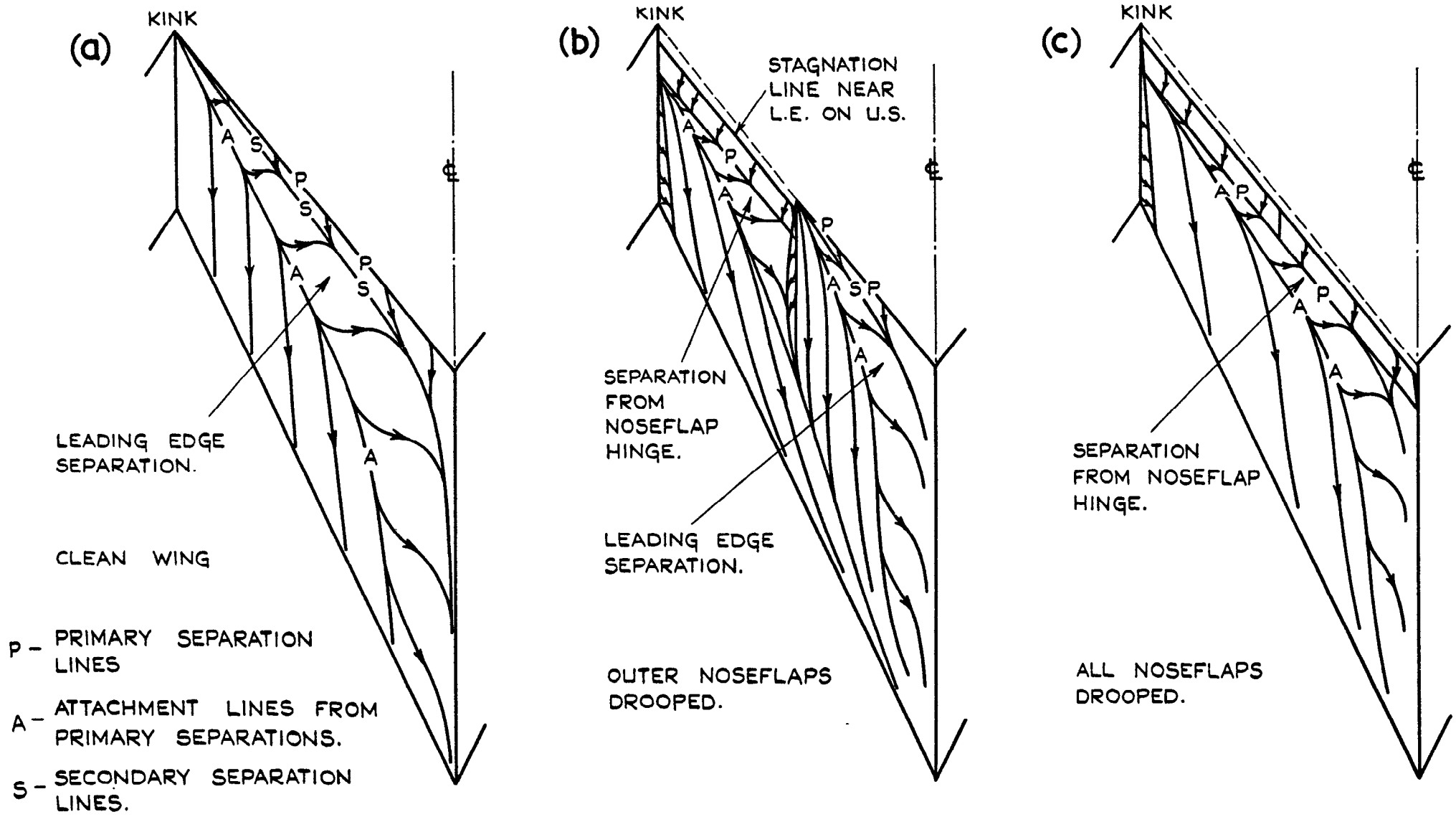

FIG. 2 (a - c) SURFACE FLOW PATTERNS ON INNER PANEL OF M-WING, WITH & WITHOUT DROOPED NOSEFLAPS, $\bar{C}_L = 0 \cdot 514$.

(a) NOSEFLAP NEUTRAL.

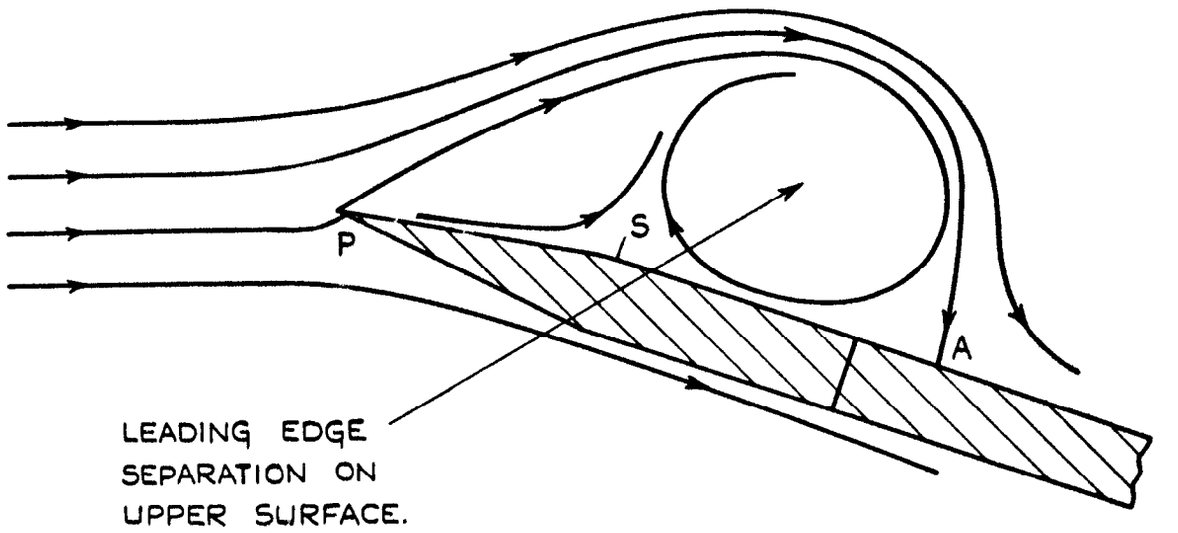

P, S – PRIMARY AND SECONDARY SEPARATION POINTS.
A – ATTACHMENT POINTS FROM PRIMARY SEPARATIONS

(b) NOSEFLAP DROOPED.

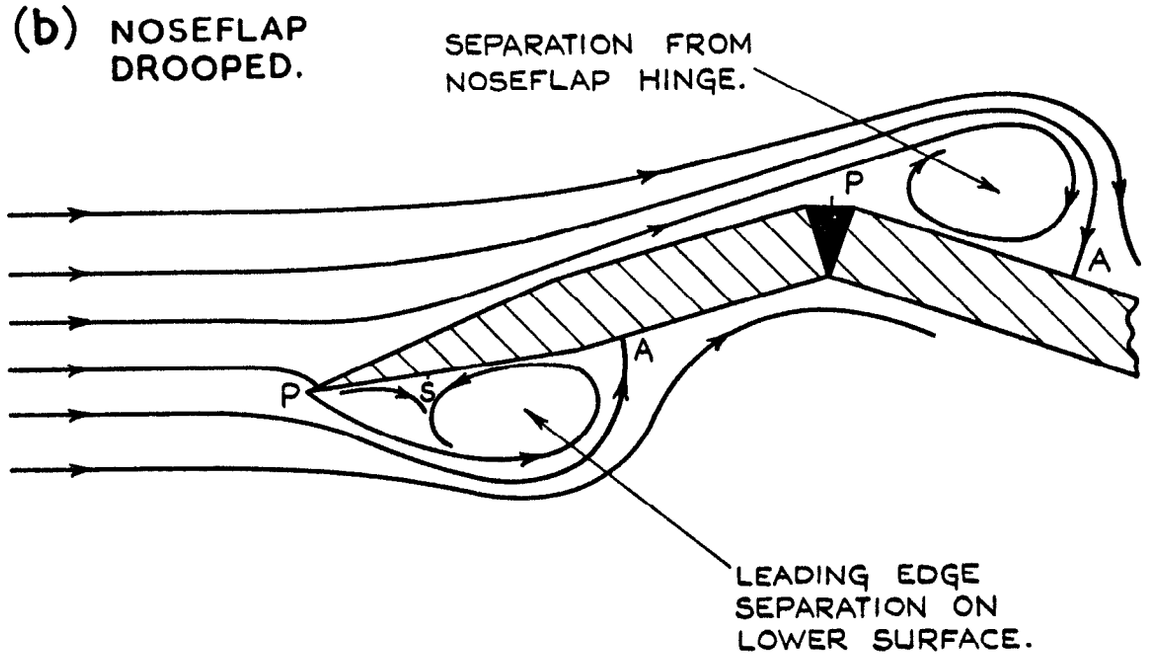

FIG. 3 (a & b) SECTIONS THROUGH FLOW NEAR LEADING EDGE OF INNER PANEL OF M-WING, WITH AND WITHOUT DROOPED NOSEFLAPS.

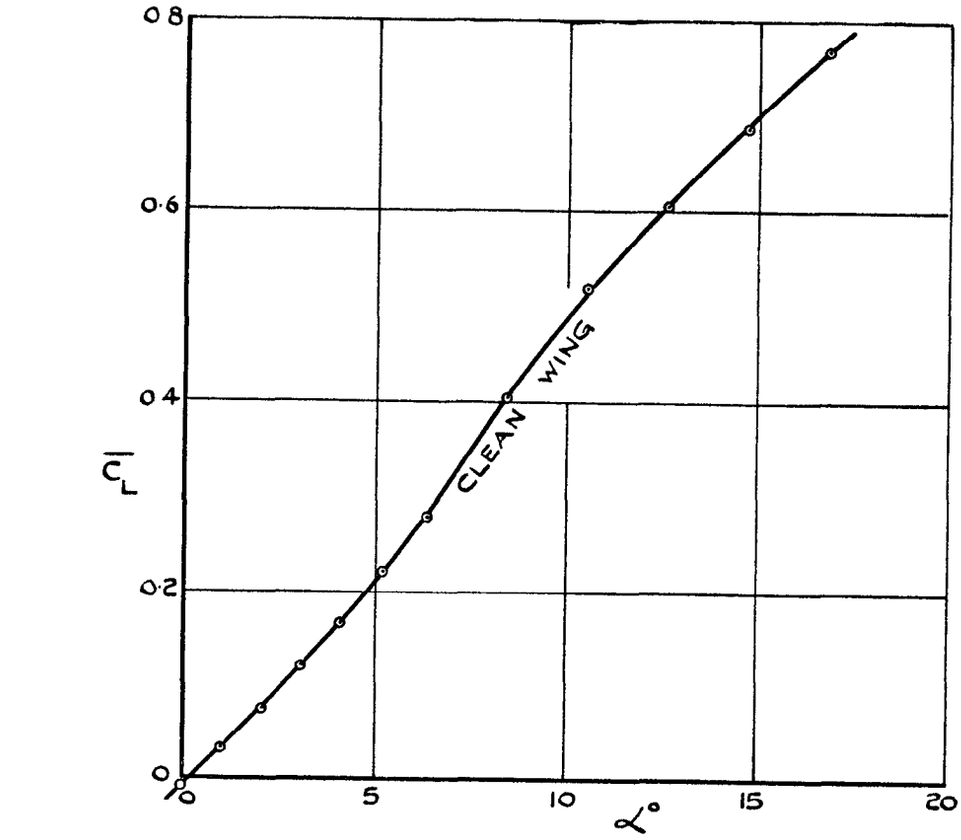

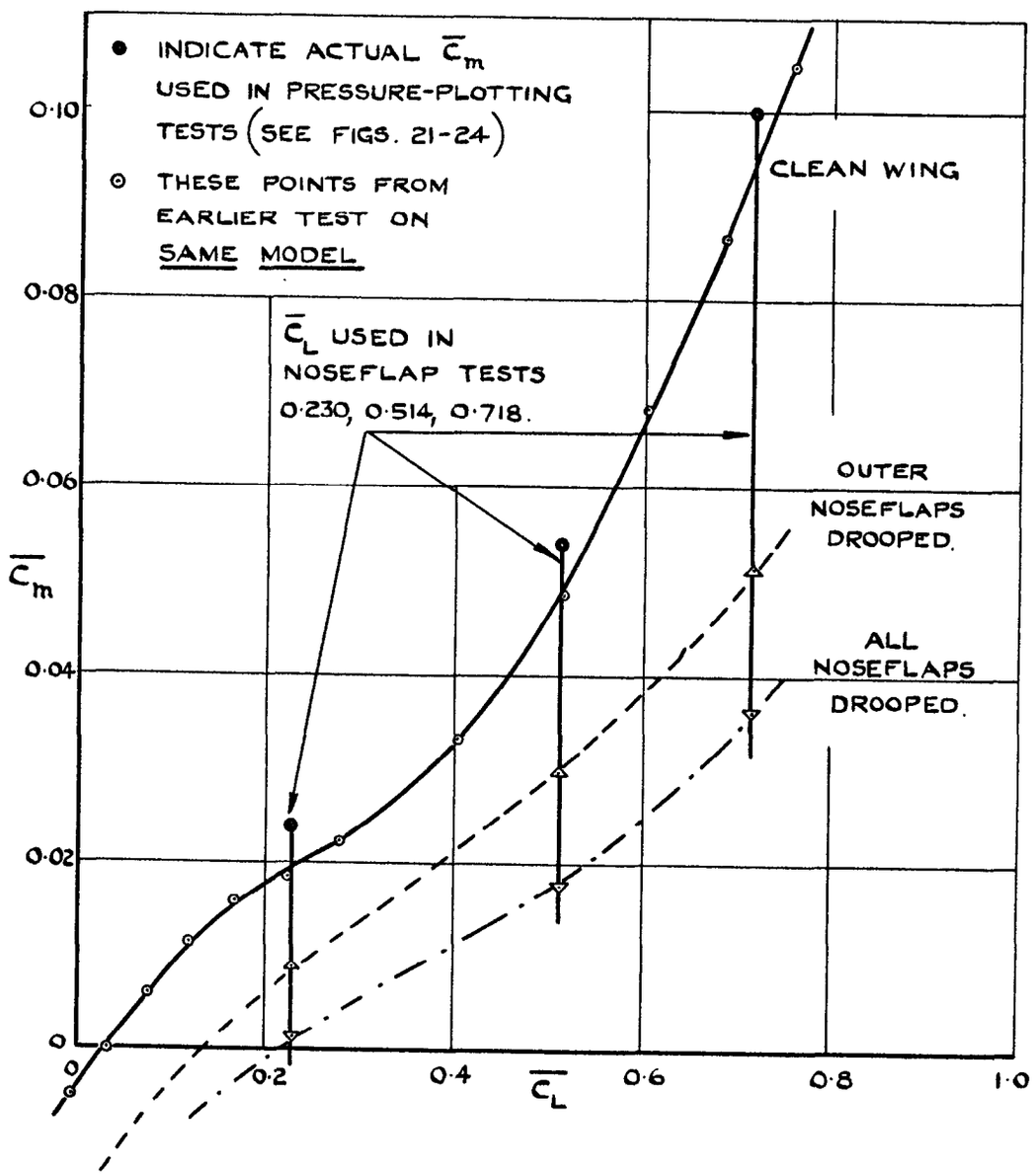

FIG. 4. LIFT & PITCHING MOMENT CHARACTERISTICS OF M-WING WITH & WITHOUT DROOPED NOSEFLAPS.

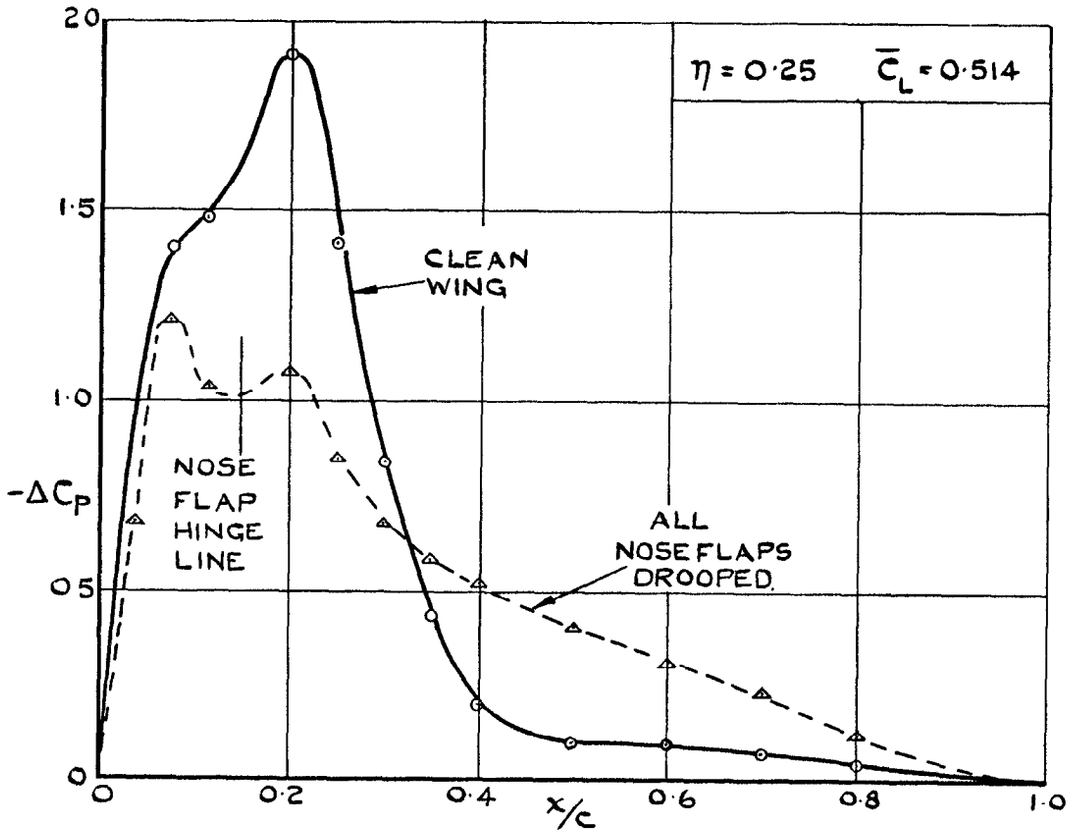

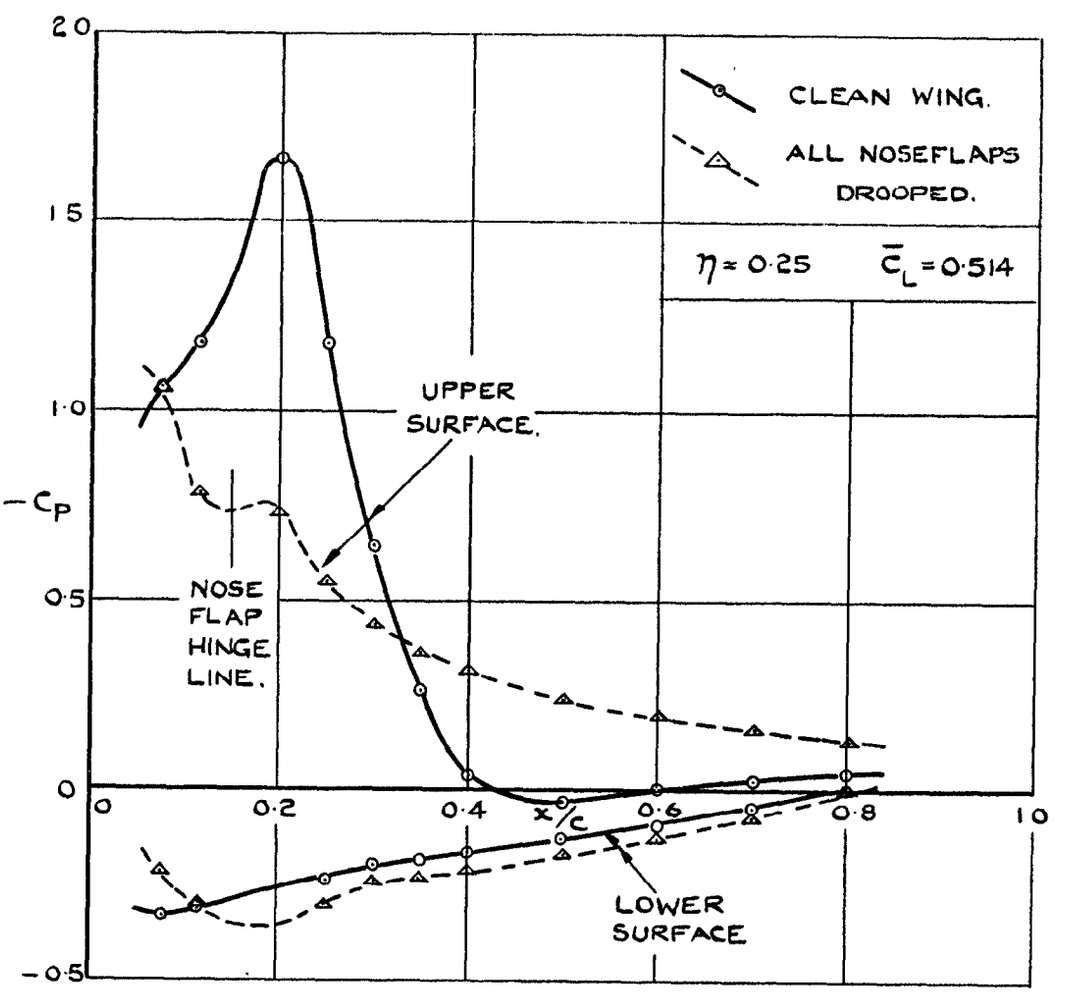

FIG.5. EFFECT OF ALL NOSEFLAPS DROOPED ON CHORDWISE DISTRIBUTION OF LOAD & SURFACE PRESSURES ON INNER PANEL OF M-WING, $\eta = 0{\cdot}25$, $\bar{C}_L = 0{\cdot}514$.

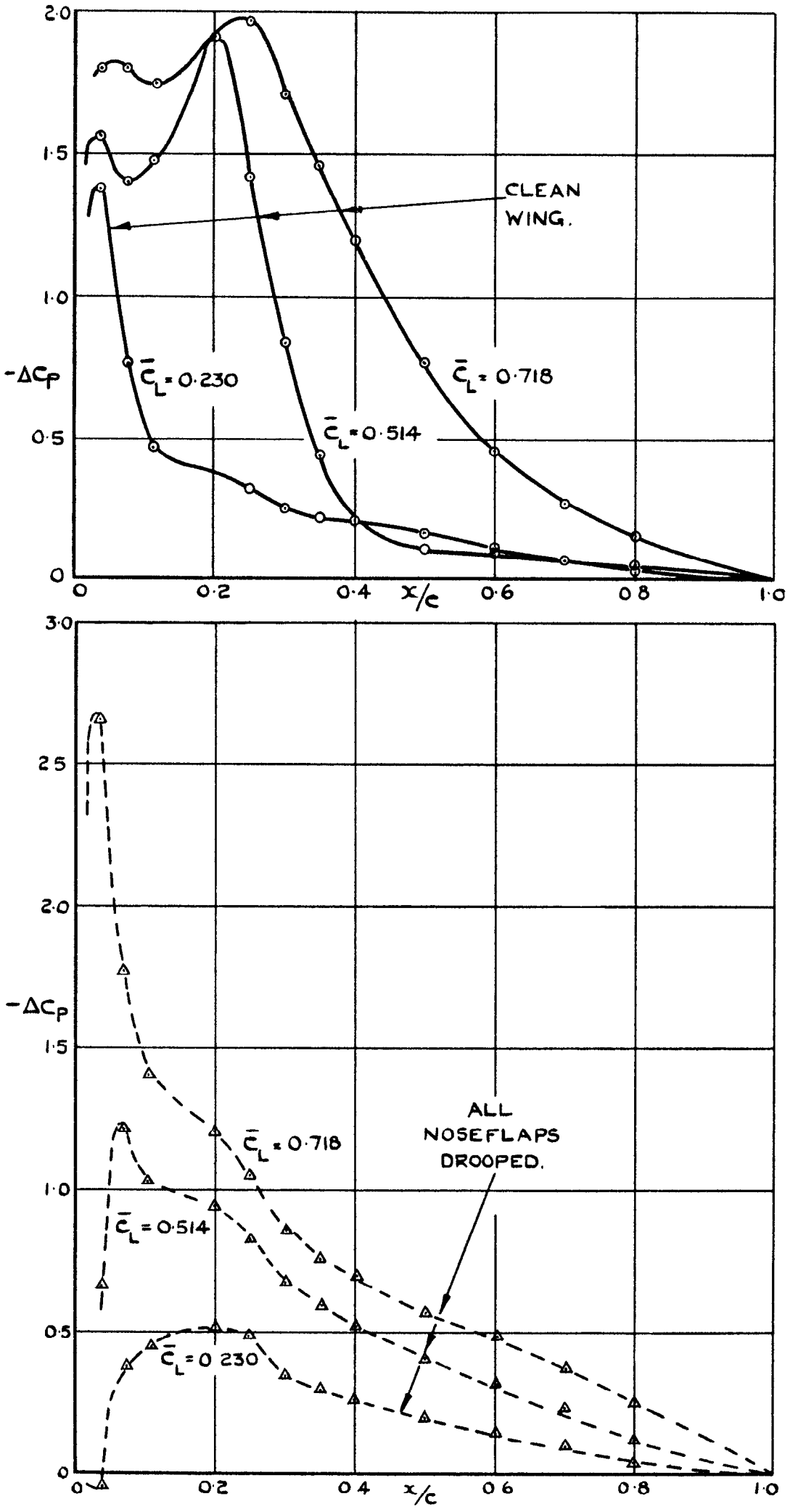

FIG. 6. EFFECT OF ALL NOSEFLAPS DROOPED ON CHORDWISE LOADING ON INNER PANEL OF M-WING, η=0·25.

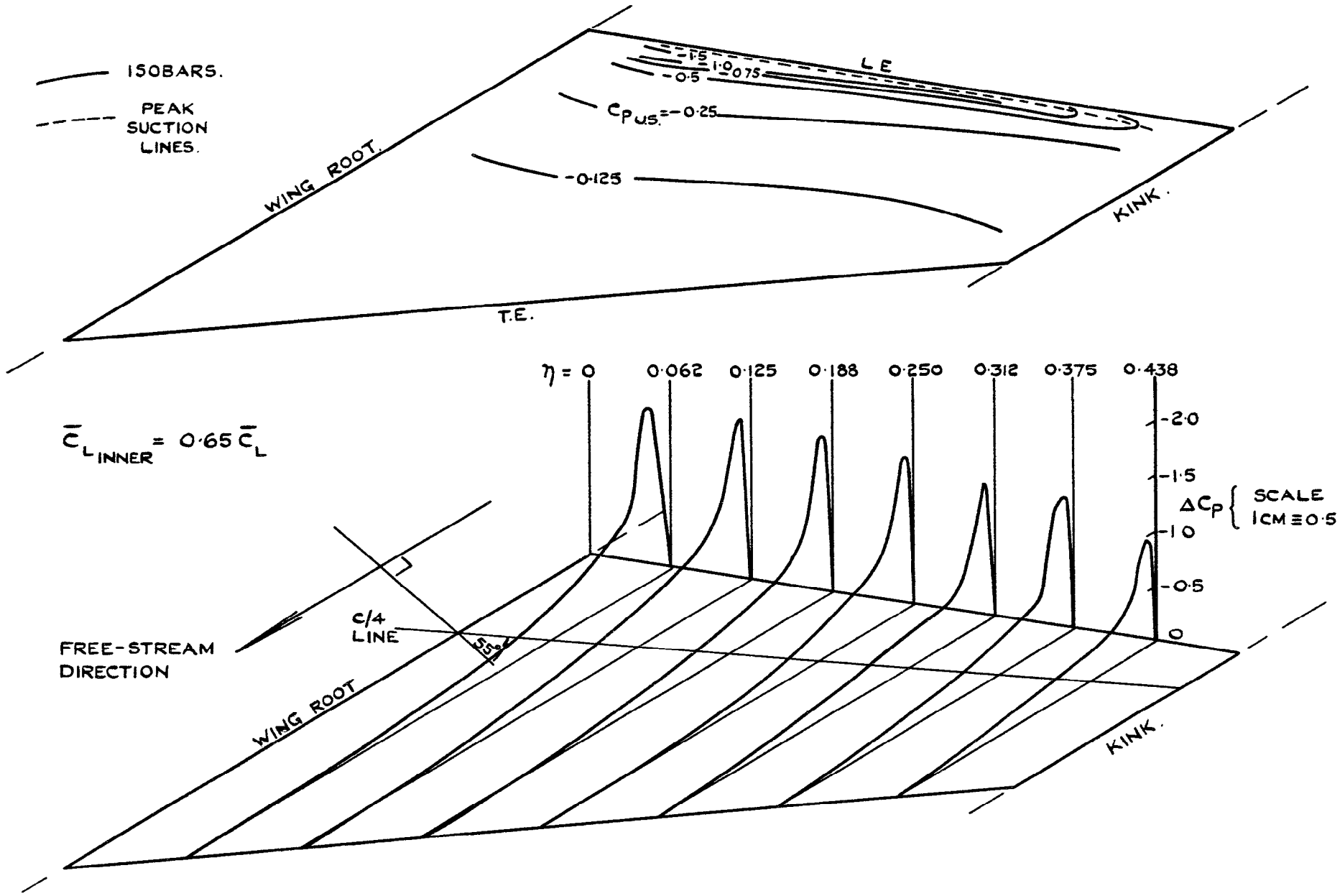

FIG. 7. DISTRIBUTIONS OF UPPER SURFACE PRESSURE & TOTAL LOAD OVER INNER PANEL OF M-WING, NOSEFLAPS NEUTRAL, $\bar{C}_L$=0·230.

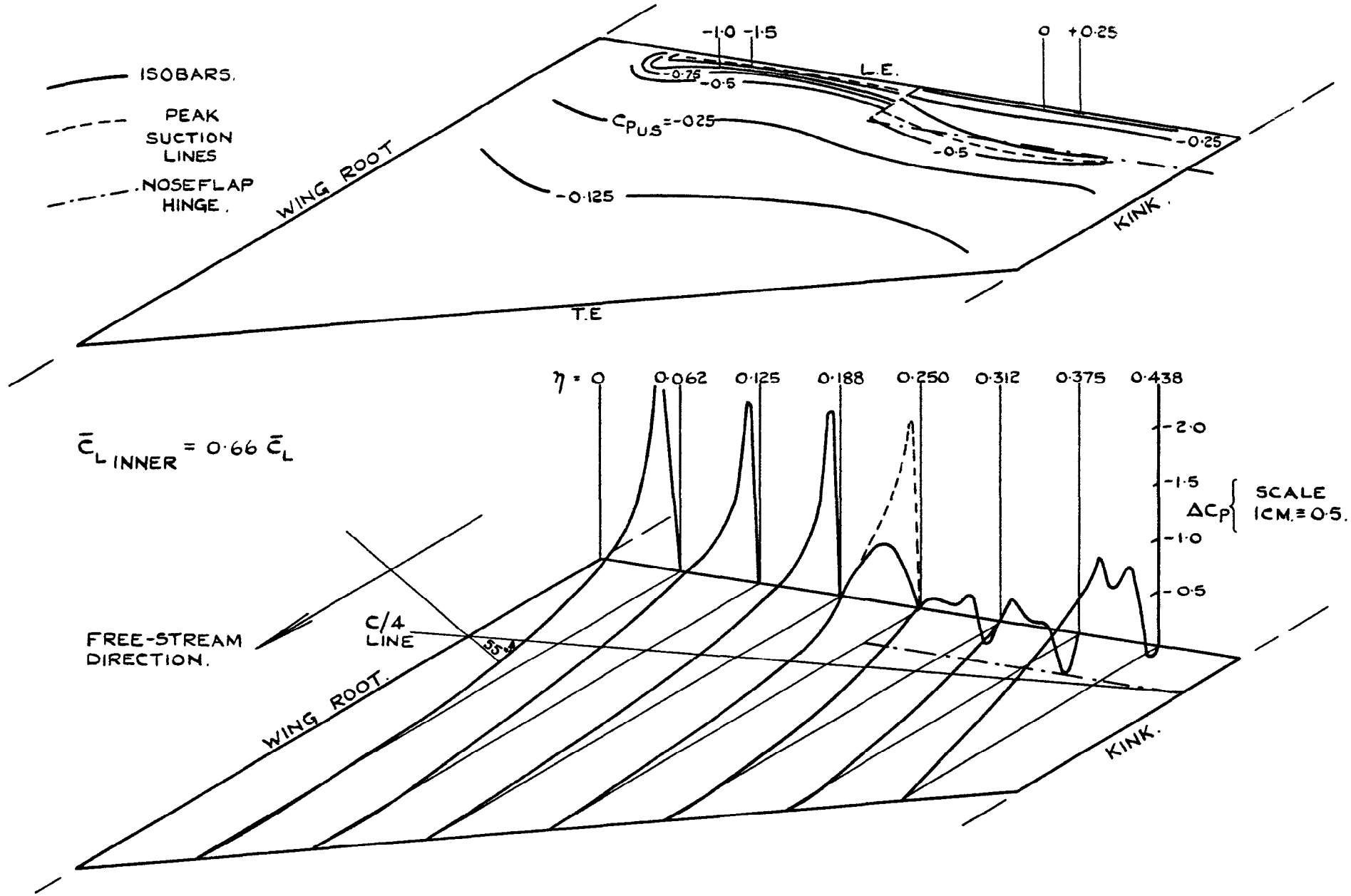

FIG. 8. DISTRIBUTIONS OF UPPER SURFACE PRESSURE & TOTAL LOAD OVER INNER PANEL OF M-WING, OUTER NOSEFLAPS DROOPED, $\bar{C}_L$=0·230.

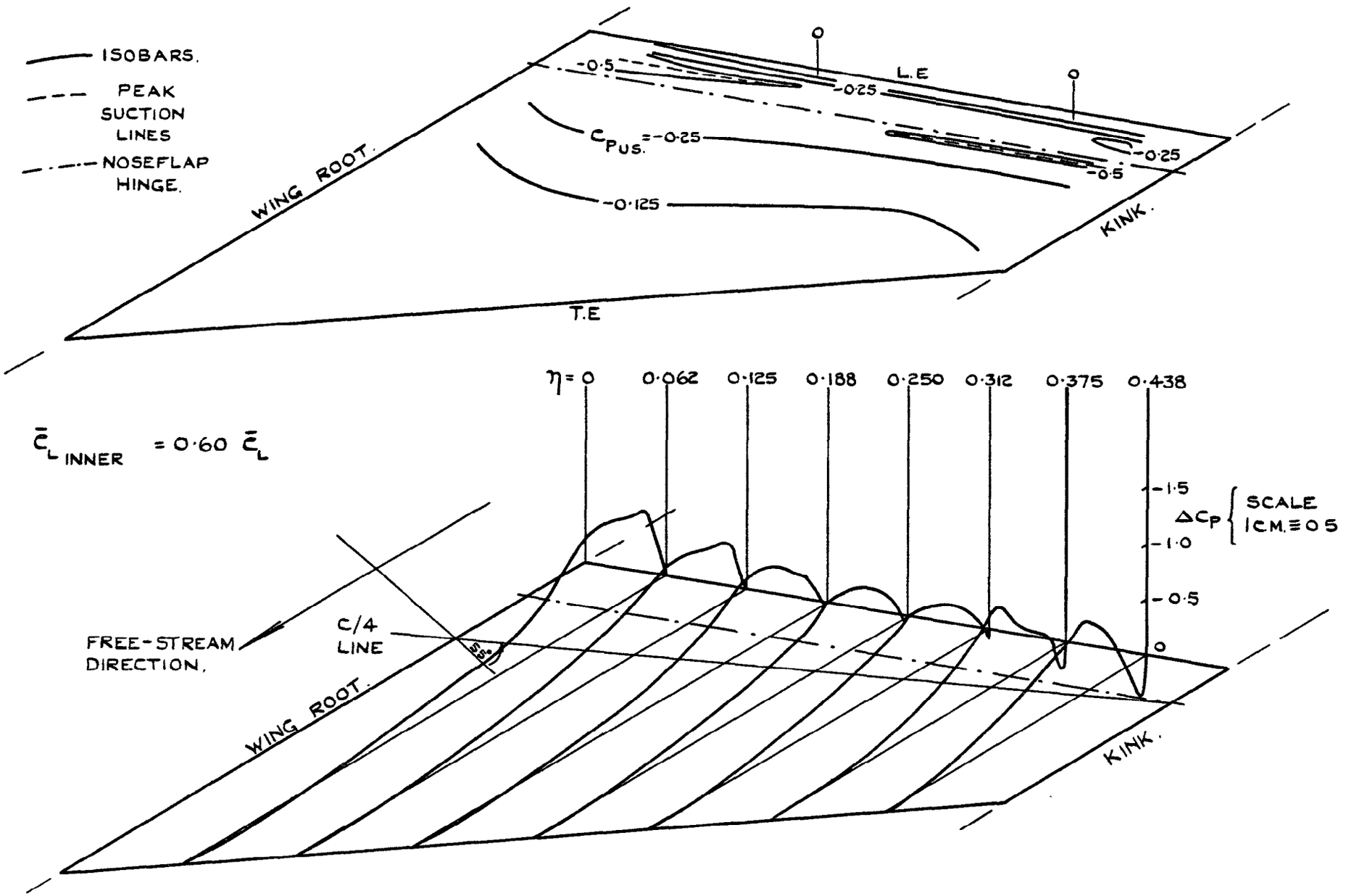

FIG. 9. DISTRIBUTIONS OF UPPER SURFACE PRESSURE & TOTAL LOAD OVER INNER PANEL OF M-WING, ALL NOSEFLAPS DROOPED, $\bar{C}_L = 0{\cdot}230$.

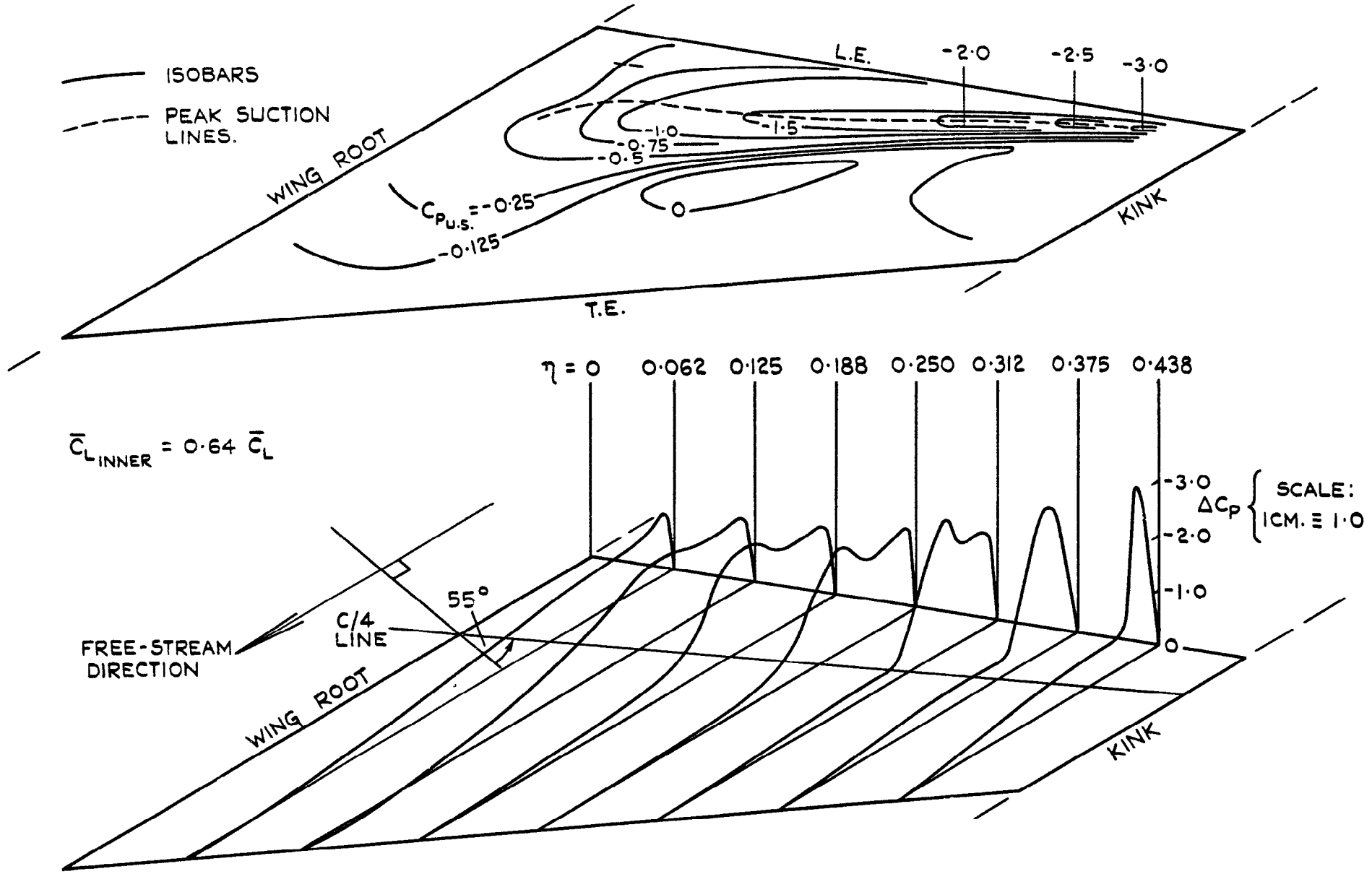

FIG. 10. DISTRIBUTIONS OF UPPER SURFACE PRESSURE & TOTAL LOAD OVER INNER PANEL OF M-WING, NOSEFLAPS NEUTRAL, $\bar{C}_L = 0{\cdot}514$.

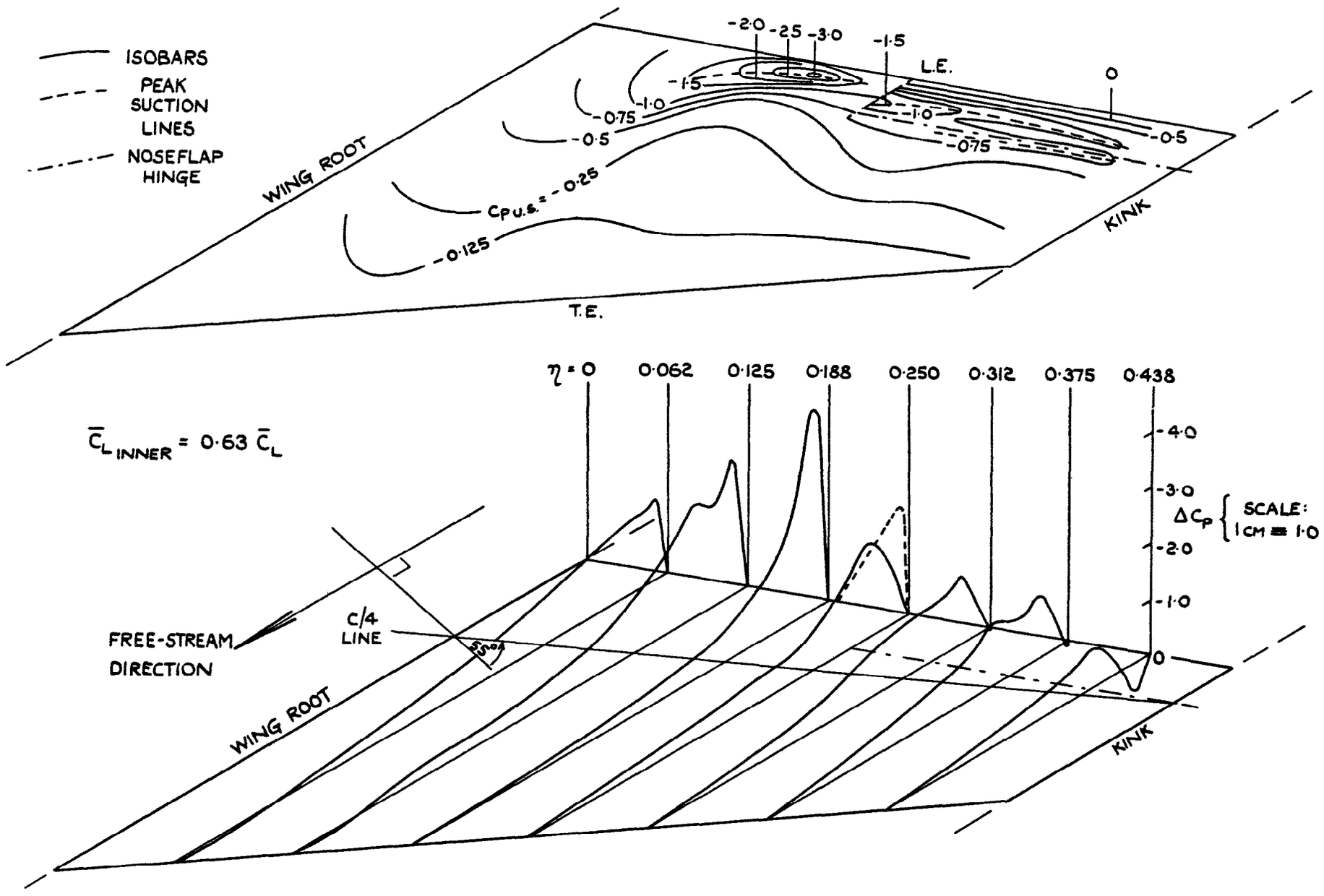

FIG.11. DISTRIBUTIONS OF UPPER SURFACE PRESSURE AND TOTAL LOAD OVER INNER PANEL OF M-WING, OUTER NOSEFLAPS DROOPED, $\bar{C}_L = 0{\cdot}514$.

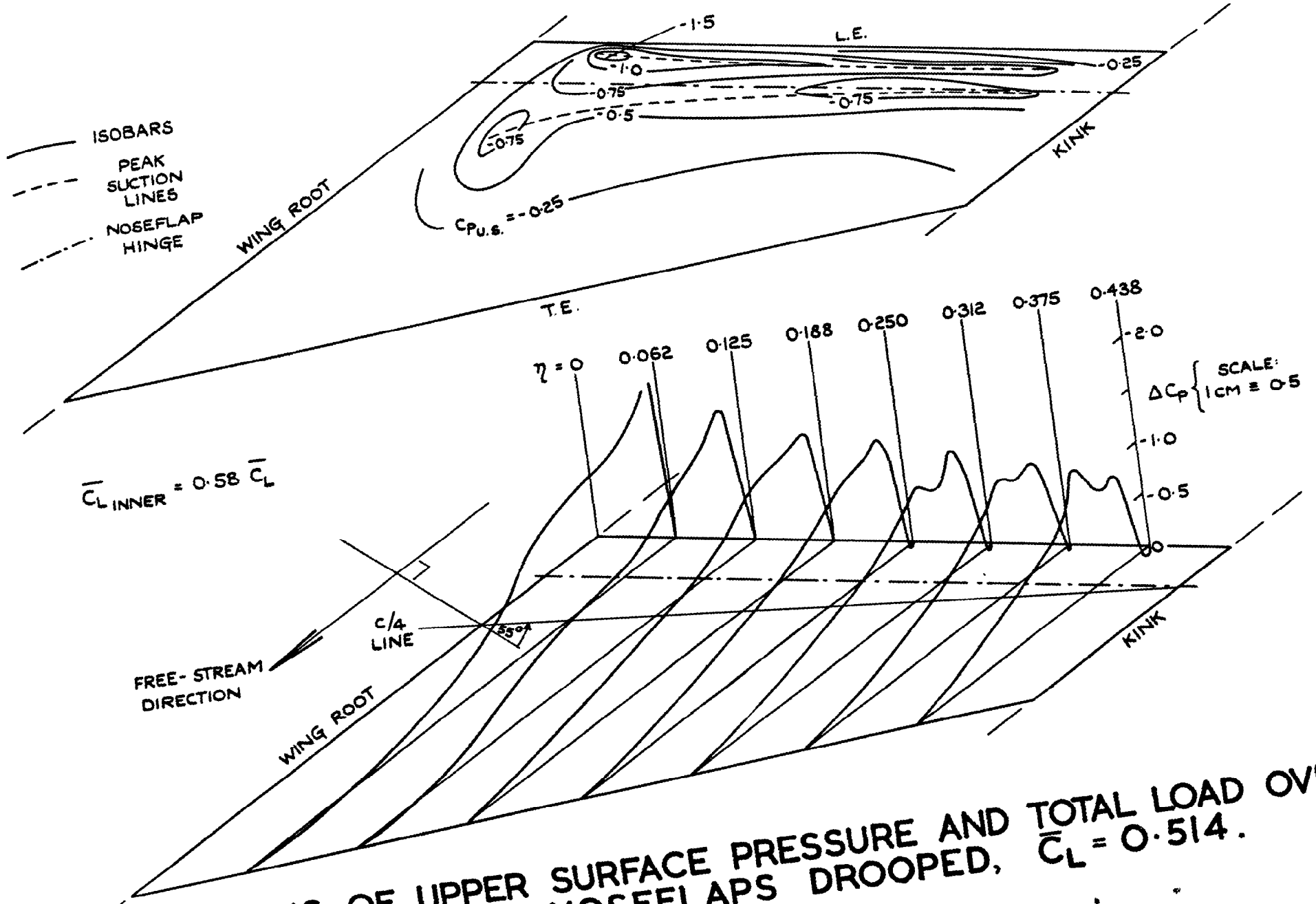

FIG.12. DISTRIBUTIONS OF UPPER SURFACE PRESSURE AND TOTAL LOAD OVER INNER PANEL OF M-WING, ALL NOSEFLAPS DROOPED, $\bar{C}_L = 0·514$.

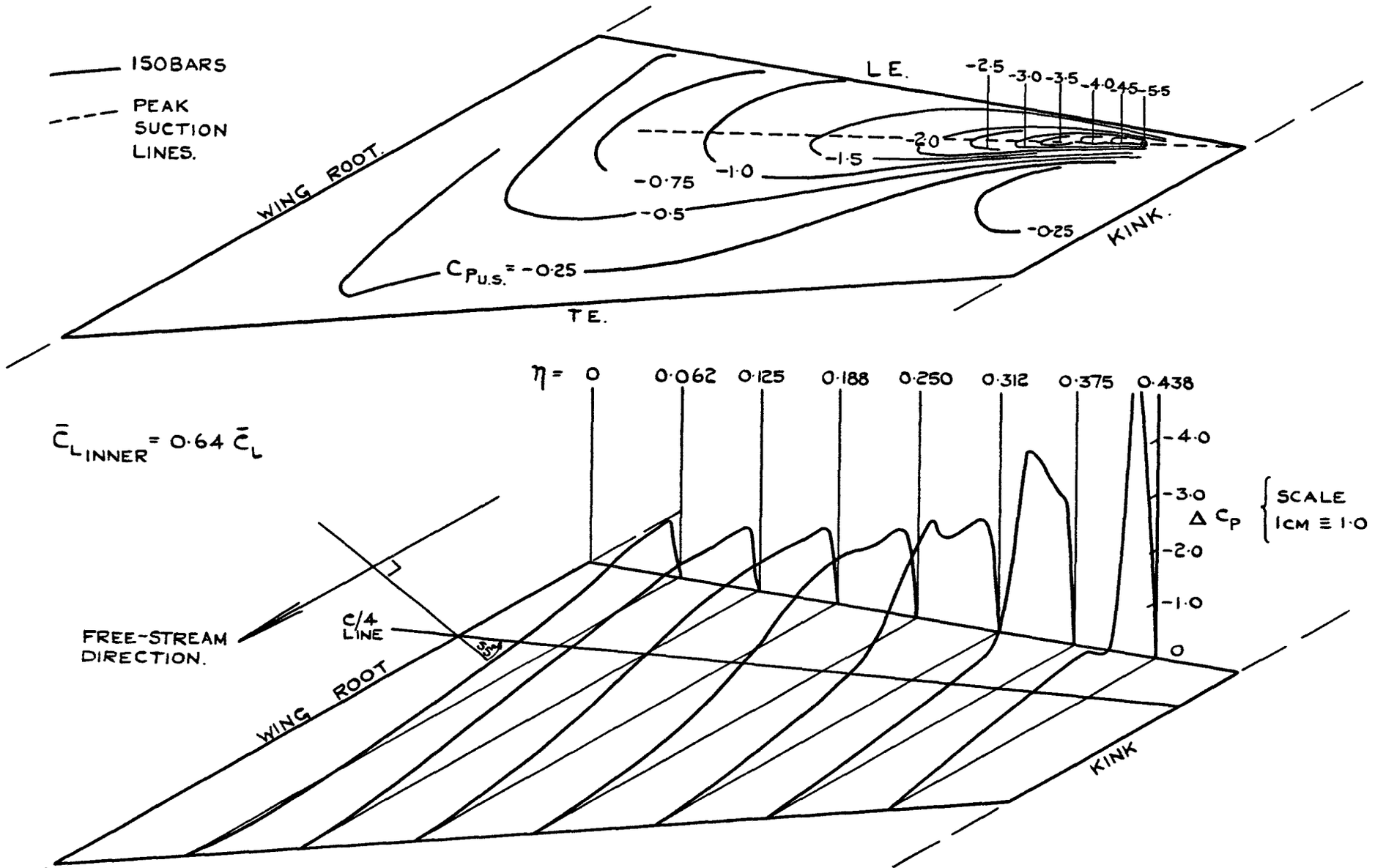

FIG. 13. DISTRIBUTIONS OF UPPER SURFACE PRESSURE & TOTAL LOAD OVER INNER PANEL OF M-WING, NOSEFLAPS NEUTRAL, $\bar{C}_L = 0·718$.

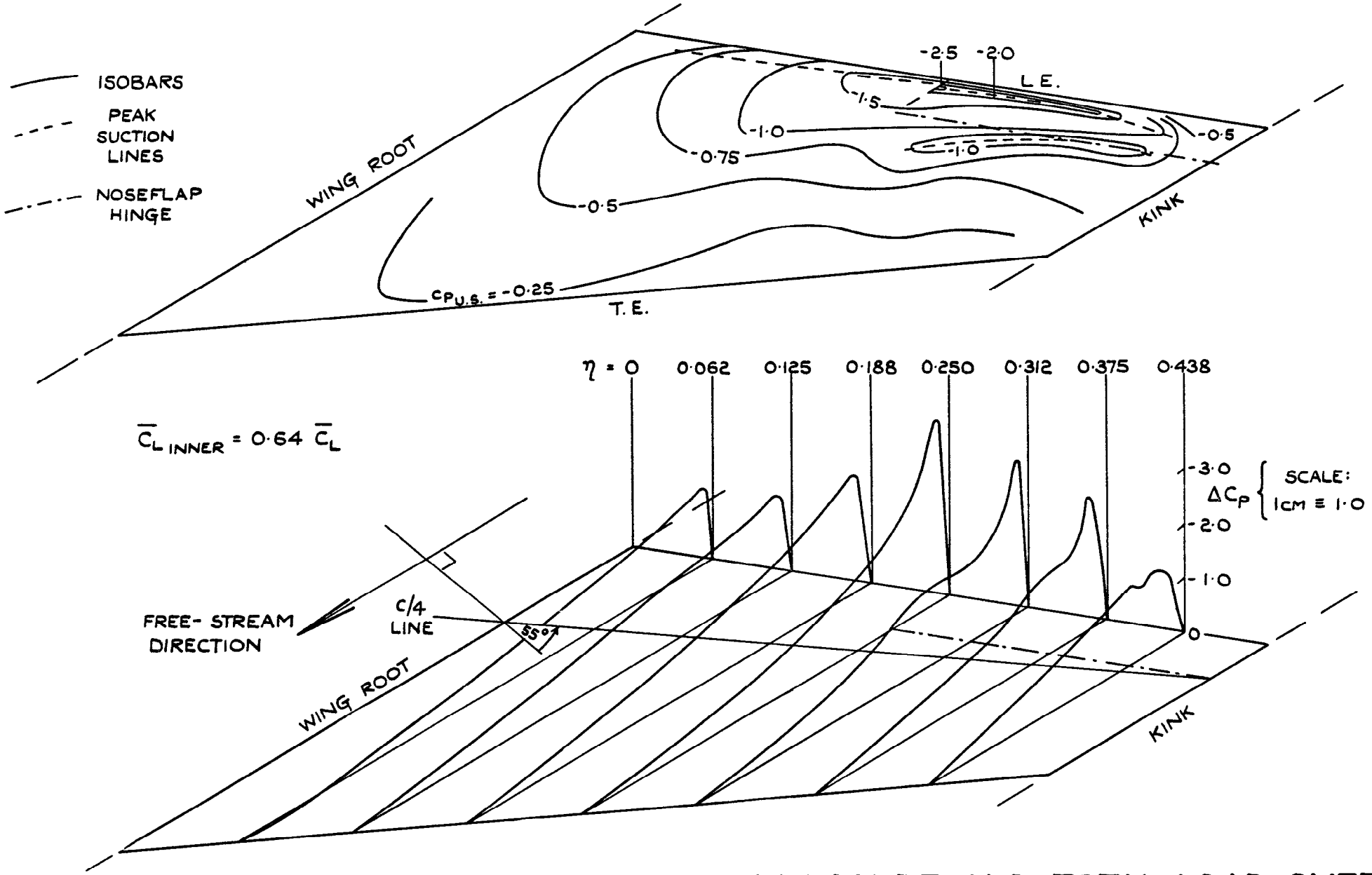

FIG. 14. DISTRIBUTIONS OF UPPER SURFACE PRESSURE AND TOTAL LOAD OVER INNER PANEL OF M-WING, OUTER NOSEFLAPS DROOPED, $\bar{C}_L = 0·718$.

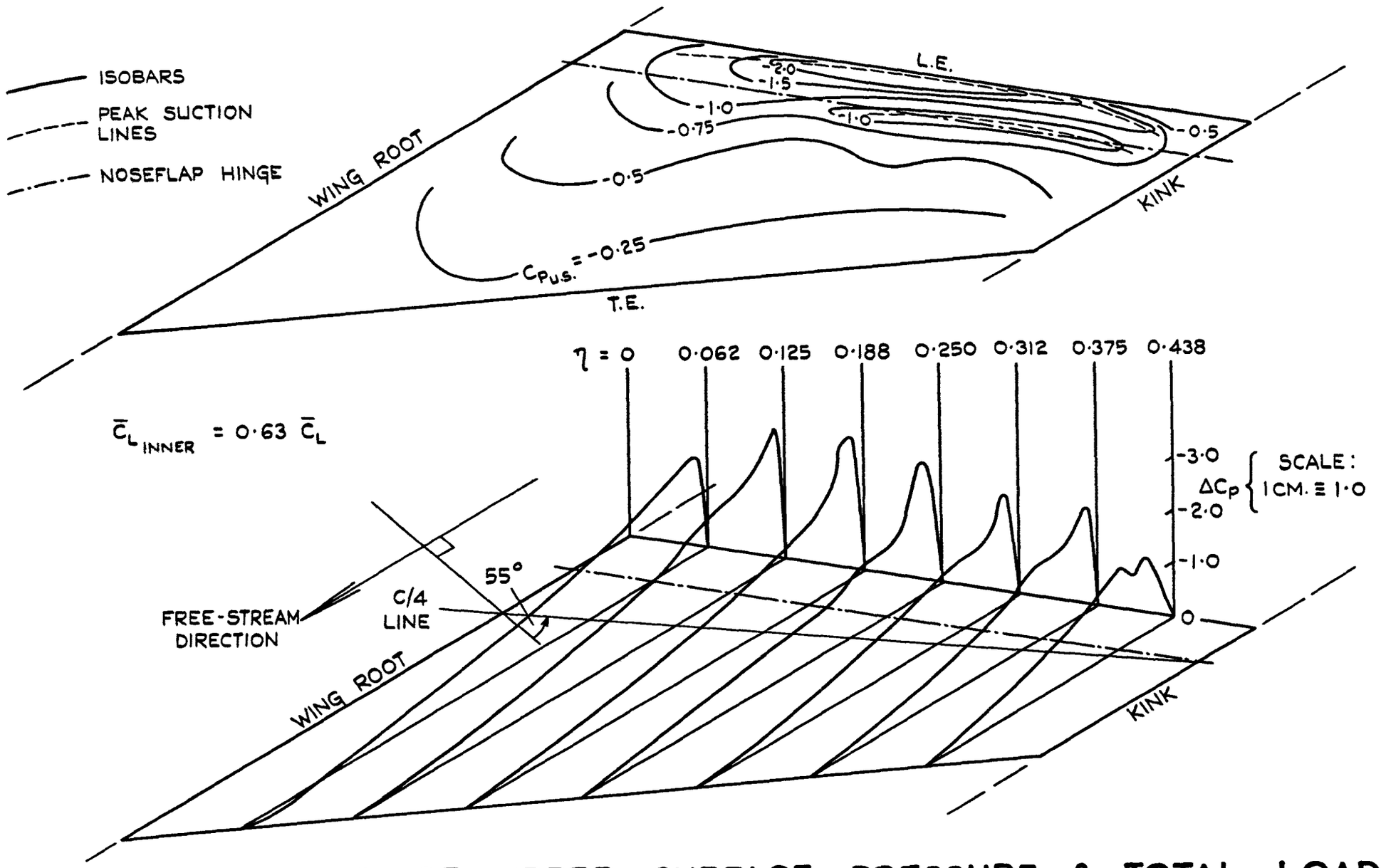

FIG. 15. DISTRIBUTIONS OF UPPER SURFACE PRESSURE & TOTAL LOAD OVER INNER PANEL OF M-WING, ALL NOSEFLAPS DROOPED, $\bar{C}_L$=0·718.

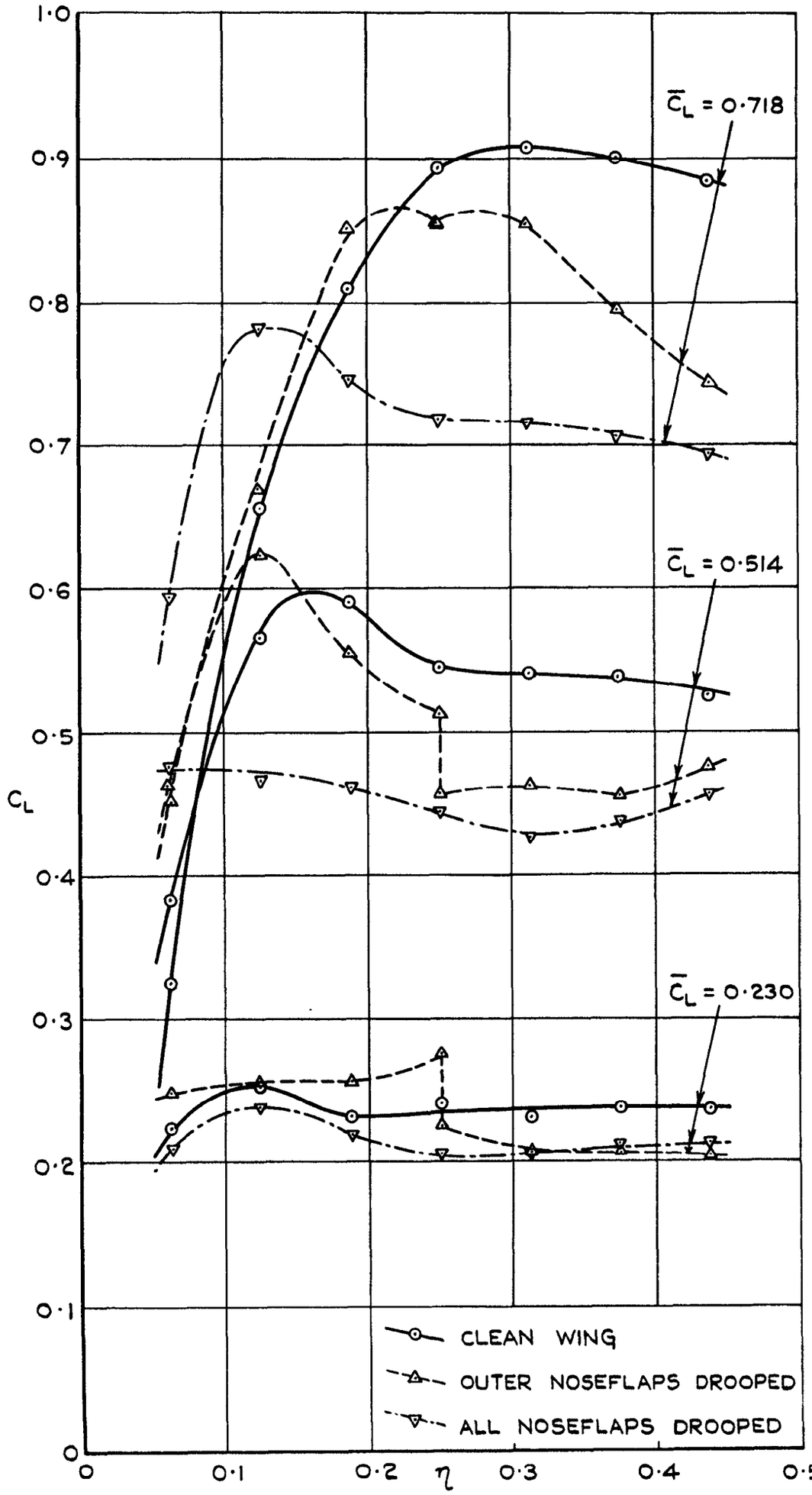

FIG. 16. SPANWISE C_L DISTRIBUTION OVER INNER PANEL OF M-WING, WITH AND WITHOUT DROOPED NOSEFLAPS.

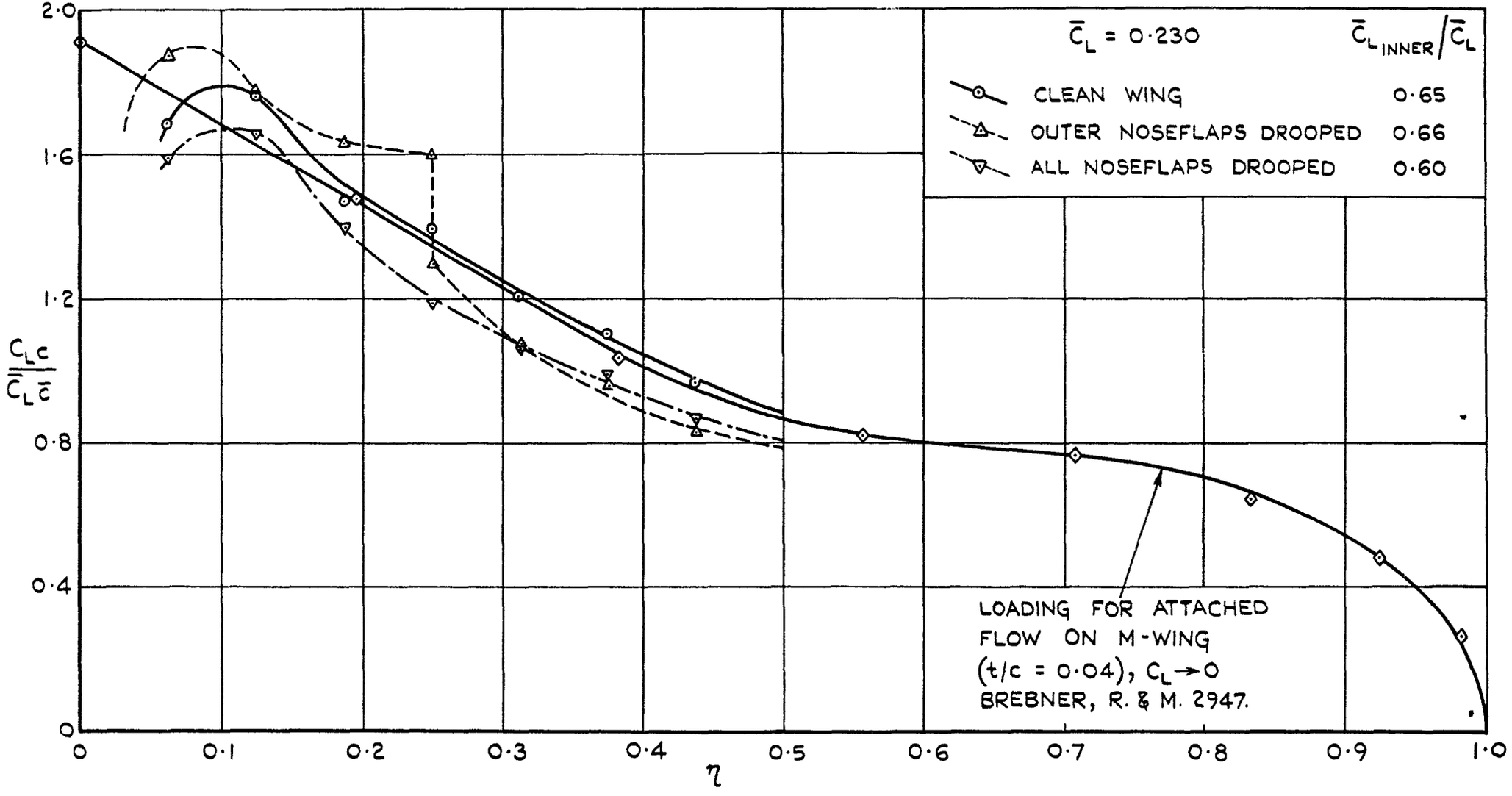

FIG. 17. SPANWISE LOADINGS ON INNER PANEL OF M-WING, WITH AND WITHOUT DROOPED NOSEFLAPS, $\bar{C}_L = 0 \cdot 230$.

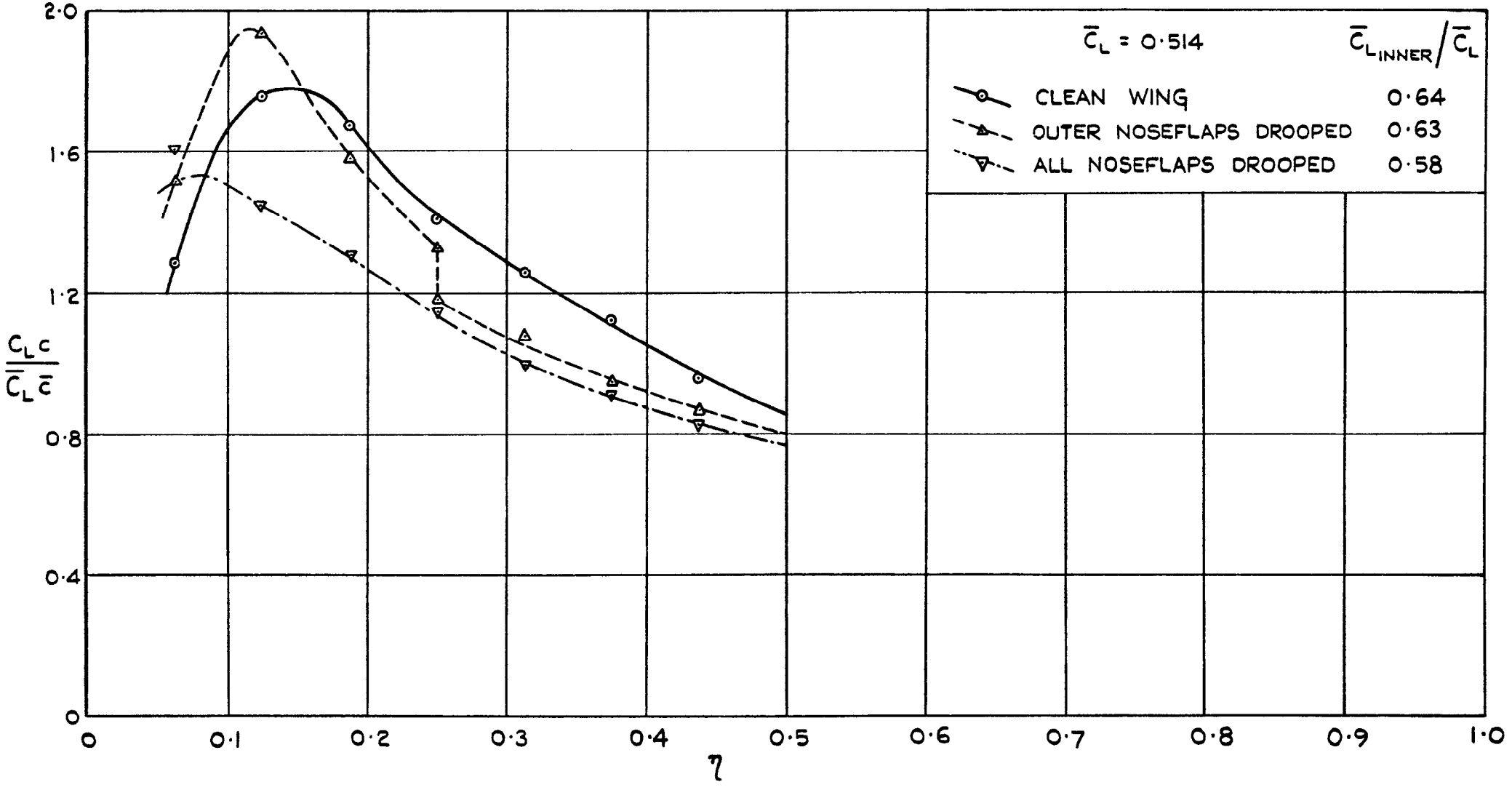

FIG. 18. SPANWISE LOADINGS ON INNER PANEL OF M-WING, WITH AND WITHOUT DROOPED NOSEFLAPS, $\bar{C}_L = 0.514$.

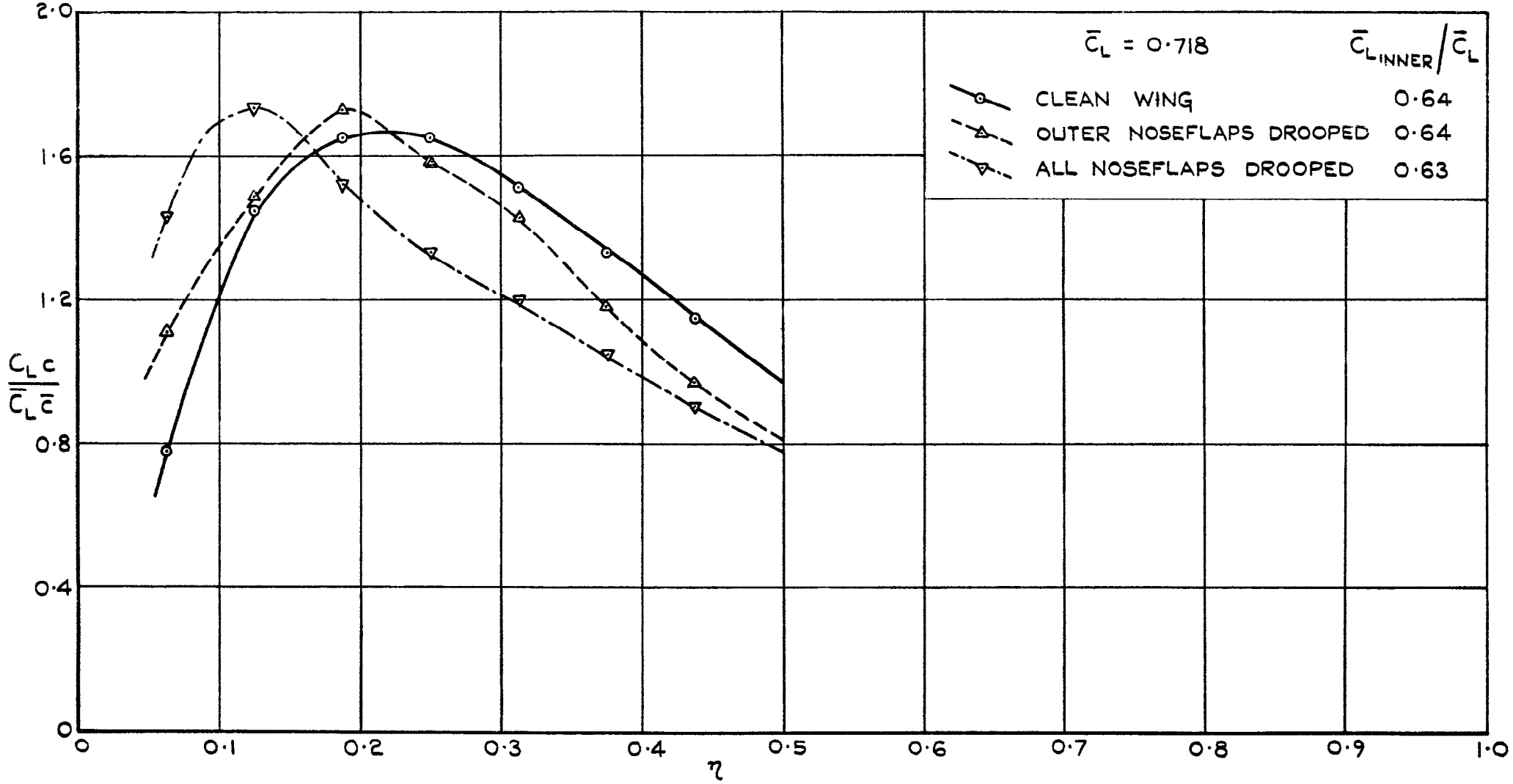

FIG. 19. SPANWISE LOADINGS ON INNER PANEL OF M-WING, WITH AND WITHOUT DROOPED NOSEFLAPS, $\bar{C}_L = 0 \cdot 718$.

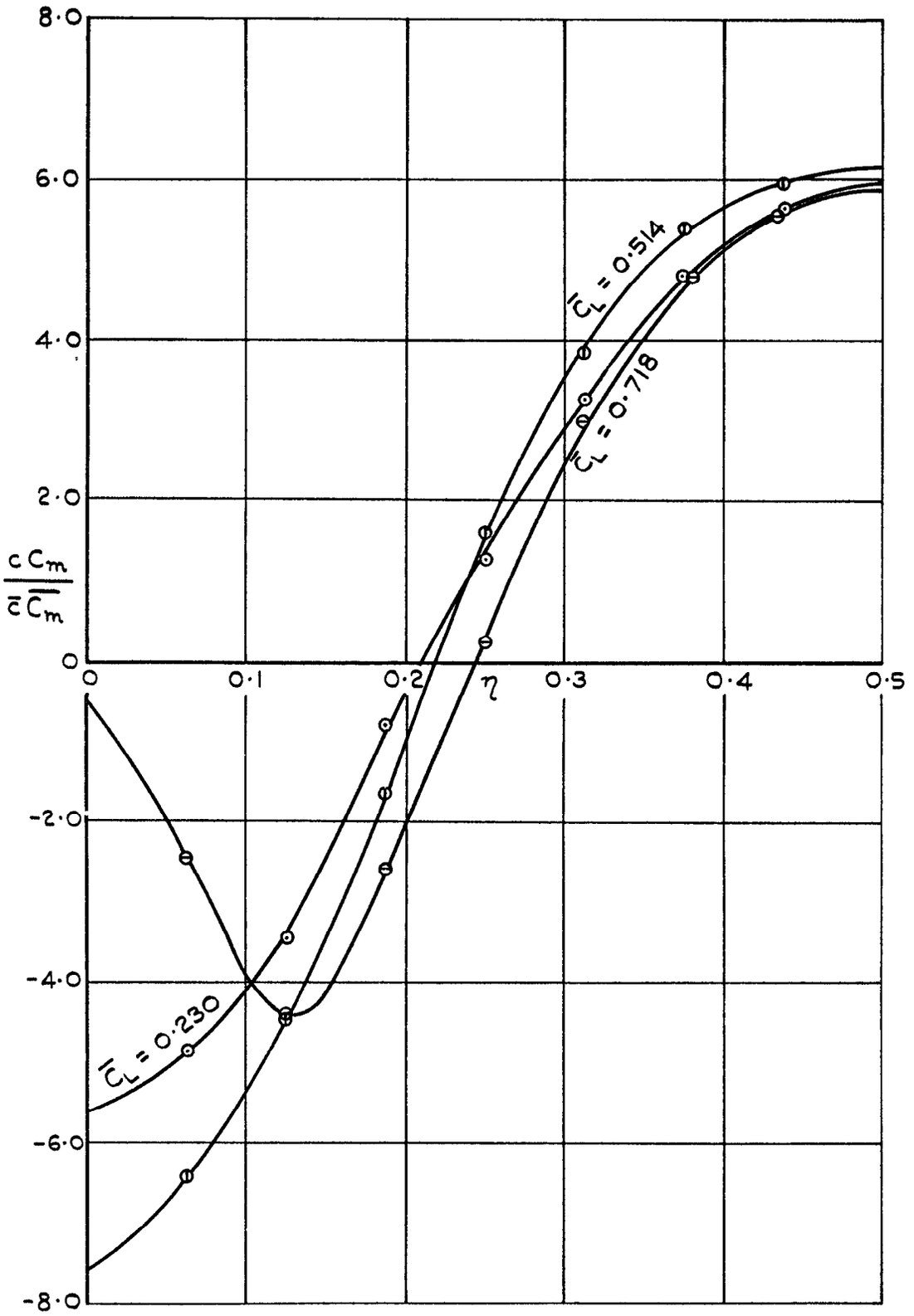

FIG. 20. SPANWISE DISTRIBUTION OF PITCHING MOMENT ACROSS INNER PANEL OF M-WING, NOSEFLAPS NEUTRAL.

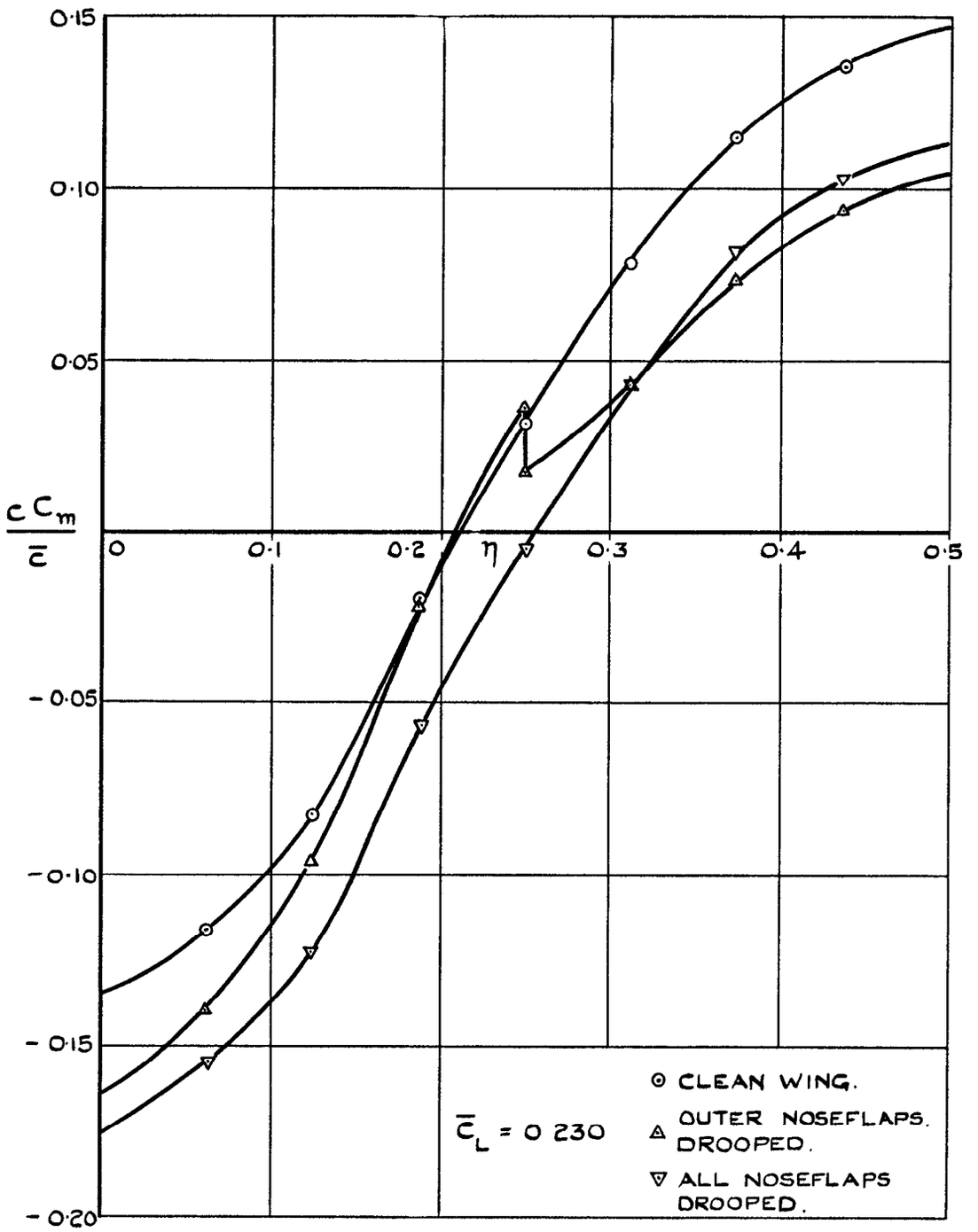

	$\bar{C}_m$	$\bar{C}_{m_{INNER}}$	$\bar{C}_{m_{OUTER}}$	$\Delta\bar{C}_m$	$\Delta\bar{C}_{m_{INNER}}$	$\Delta\bar{C}_{m_{OUTER}}$
CLEAN WING	0.0239	0·0092	0·0147			
OUTER NOSEFLAPS DROOPED.	0·0092	-0·0032	0·0124	-0·0147	-0·0124	-0·0023
ALL NOSEFLAPS DROOPED.	0·0014	-0·0090	0·0104	-0·0225	-0·0182	-0·0043

FIG.21. EFFECT OF NOSEFLAP DROOP ON THE SPANWISE DISTRIBUTION OF PITCHING MOMENT OVER INNER PANEL OF M-WING, $\bar{C}_L$=0·230.

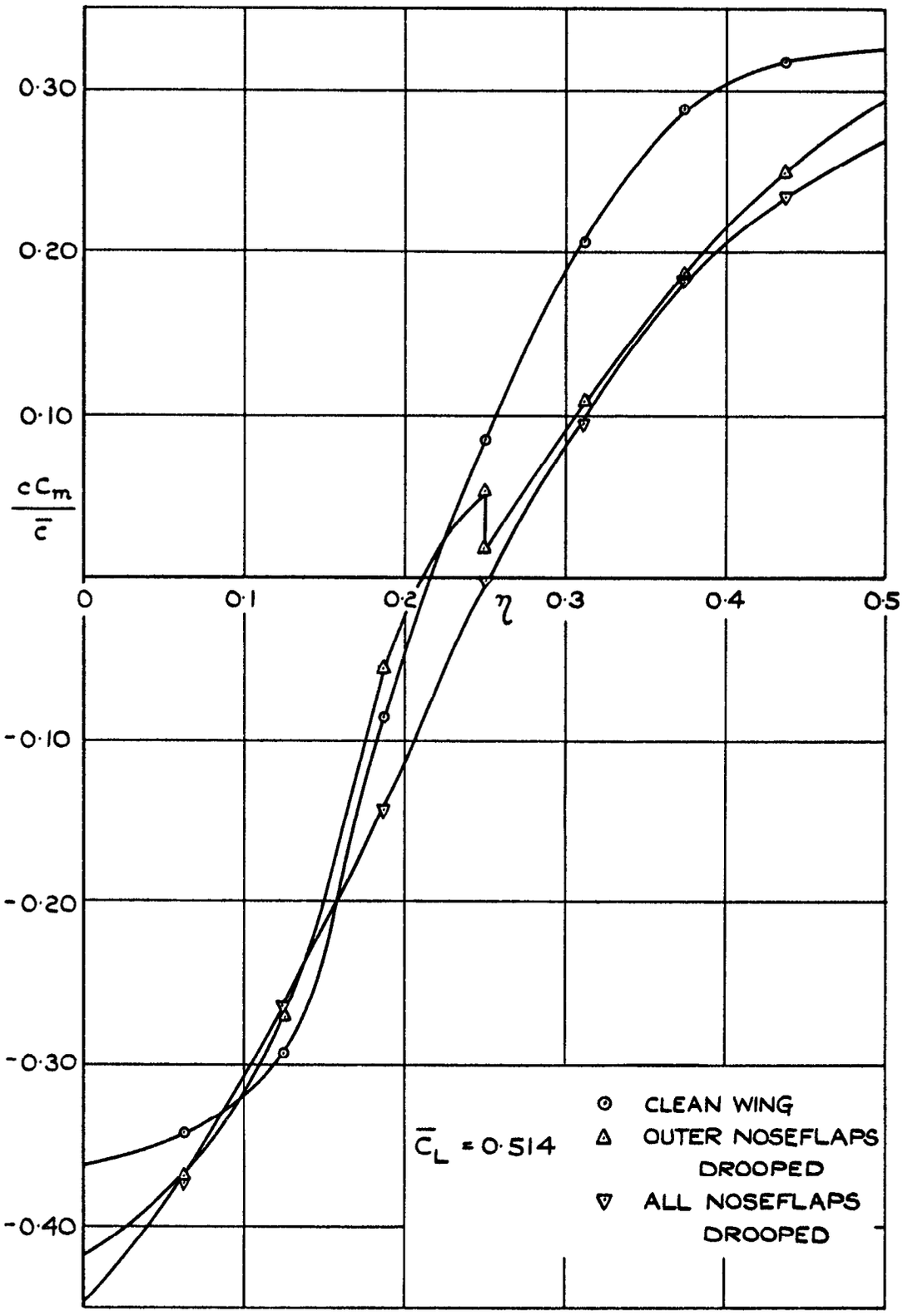

	$\bar{C}_m$	$\bar{C}_{m\,INNER}$	$\bar{C}_{m\,OUTER}$	$\Delta\bar{C}_m$	$\Delta\bar{C}_{m\,INNER}$	$\Delta\bar{C}_{m\,OUTER}$
CLEAN WING	0·0535	0·0102	0·0433			
OUTER NOSEFLAPS DROOPED	0·0298	-0·0110	0·0398	-0·0237	-0·0222	-0·0035
ALL NOSEFLAPS DROOPED	0·0174	-0·0215	0·0389	-0·0361	-0·0317	-0·0044

FIG. 22. EFFECT OF NOSEFLAP DROOP ON THE SPANWISE DISTRIBUTION OF PITCHING MOMENT OVER INNER PANEL OF M-WING, $\bar{C}_L$ = 0·514.

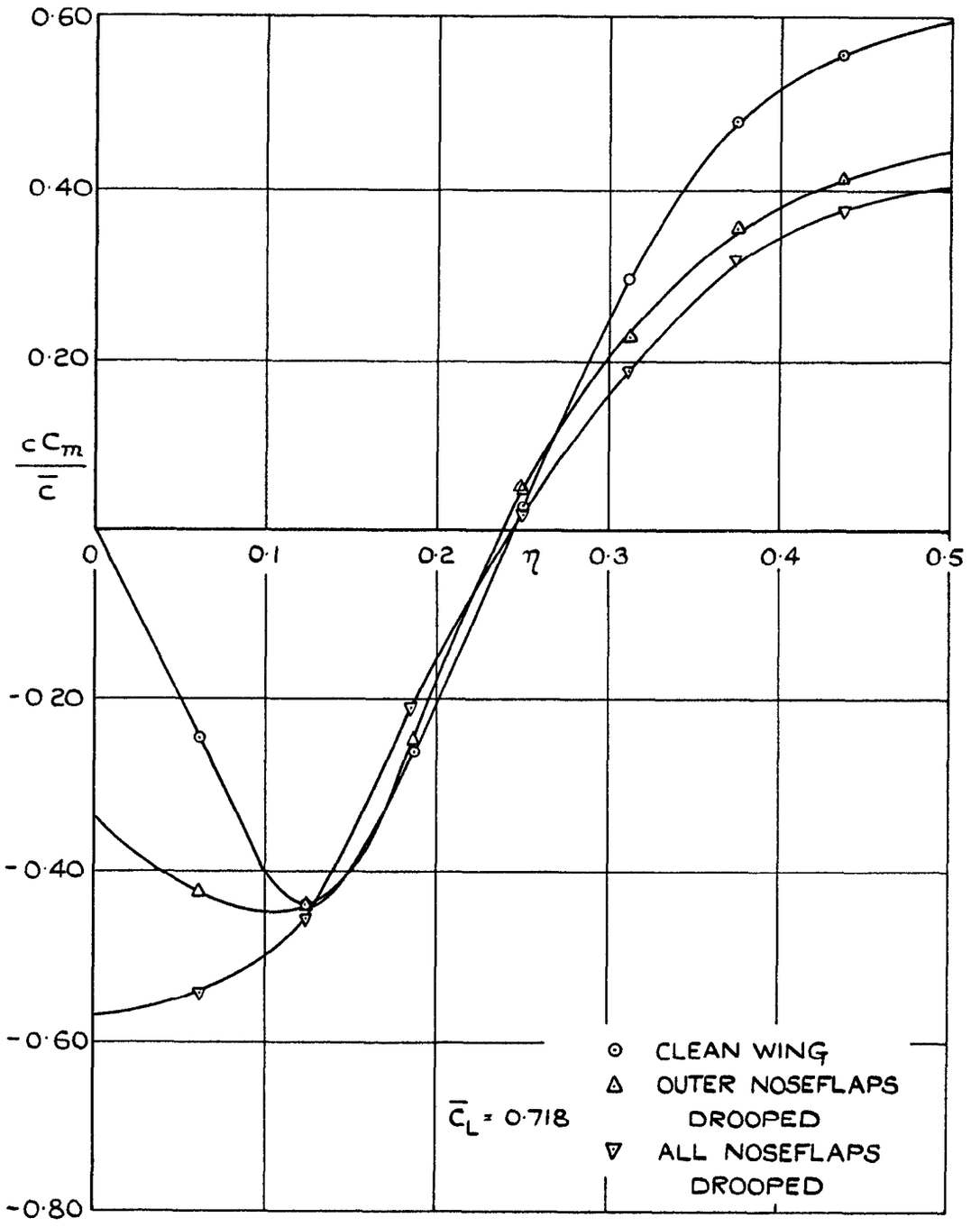

	$\bar{C}_m$	$\bar{C}_{m_{INNER}}$	$\bar{C}_{m_{OUTER}}$	$\Delta\bar{C}_m$	$\Delta\bar{C}_{m_{INNER}}$	$\Delta C_{m_{OUTER}}$
CLEAN WING	0·1002	0·0430	0·0572			
OUTER NOSEFLAPS DROOPED	0·0513	-0·0001	0·0514	-0·0489	-0·0431	-0·0058
ALL NOSEFLAPS DROOPED	0·0359	-0·0240	0·0599	-0·0643	-0·0670	0·0027

FIG. 23. EFFECT OF NOSEFLAP DROOP ON THE SPANWISE DISTRIBUTION OF PITCHING MOMENT OVER INNER PANEL OF M-WING, $\bar{C}_L = 0·718$.

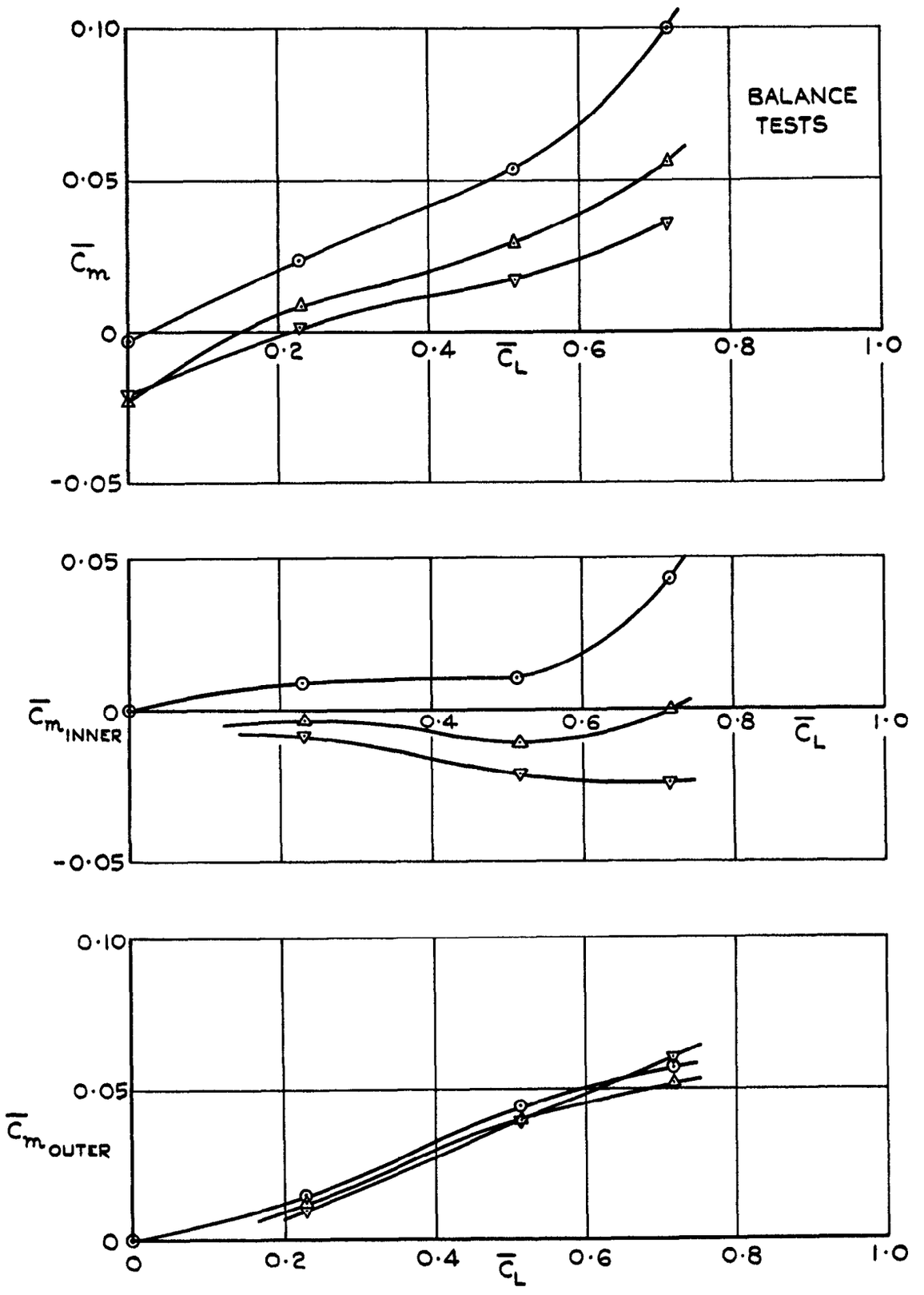

SYMBOLS ⊙ CLEAN WING
△ OUTER NOSEFLAPS DROOPED
▽ ALL NOSEFLAPS DROOPED

FIG. 24. EFFECT OF NOSEFLAP DROOP ON OVERALL PITCHING MOMENTS ON M-WING.

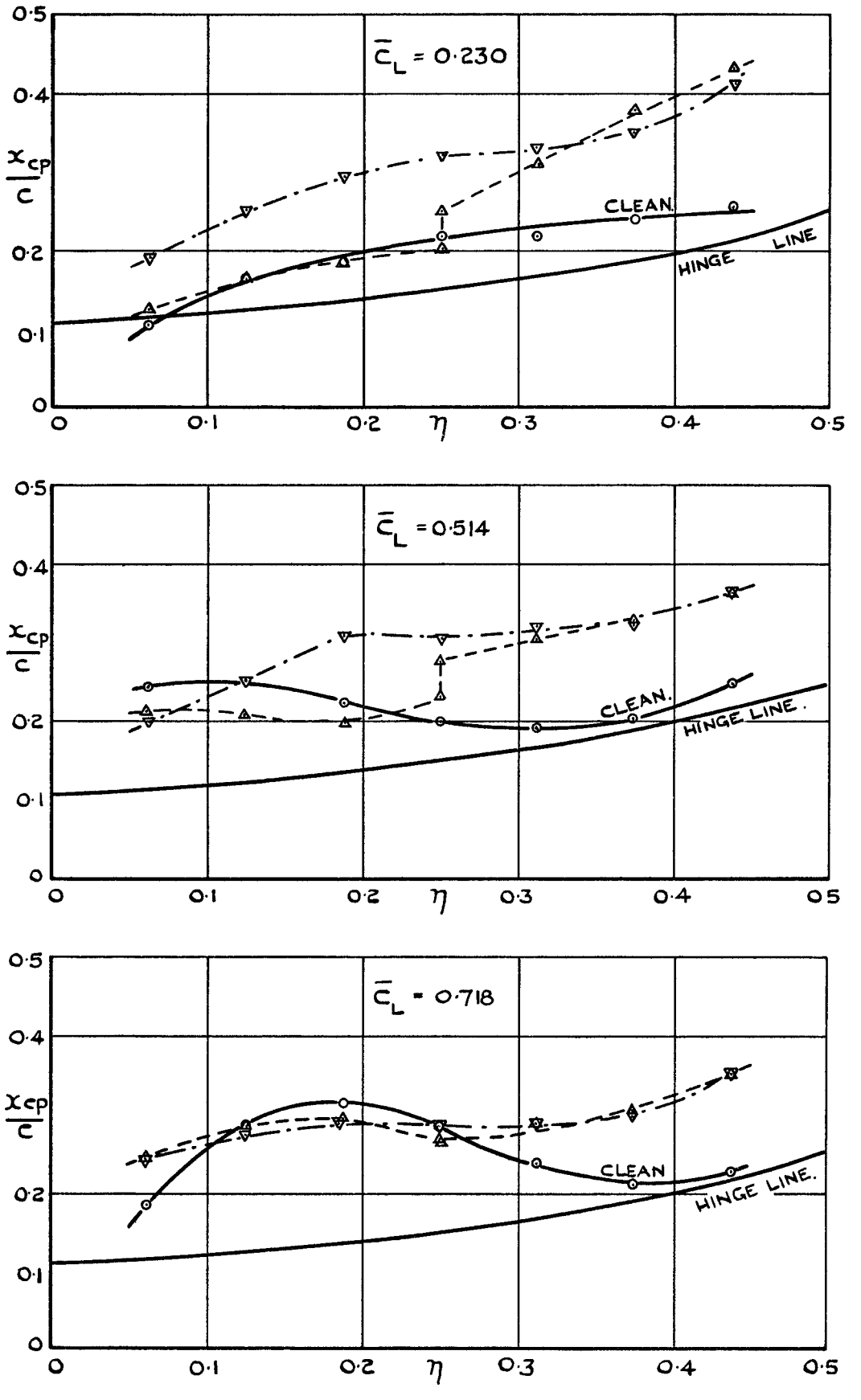

FIG.25. CENTRE OF PRESSURE POSITION AS A FRACTION OF LOCAL CHORD ON INNER PANEL OF M-WING.

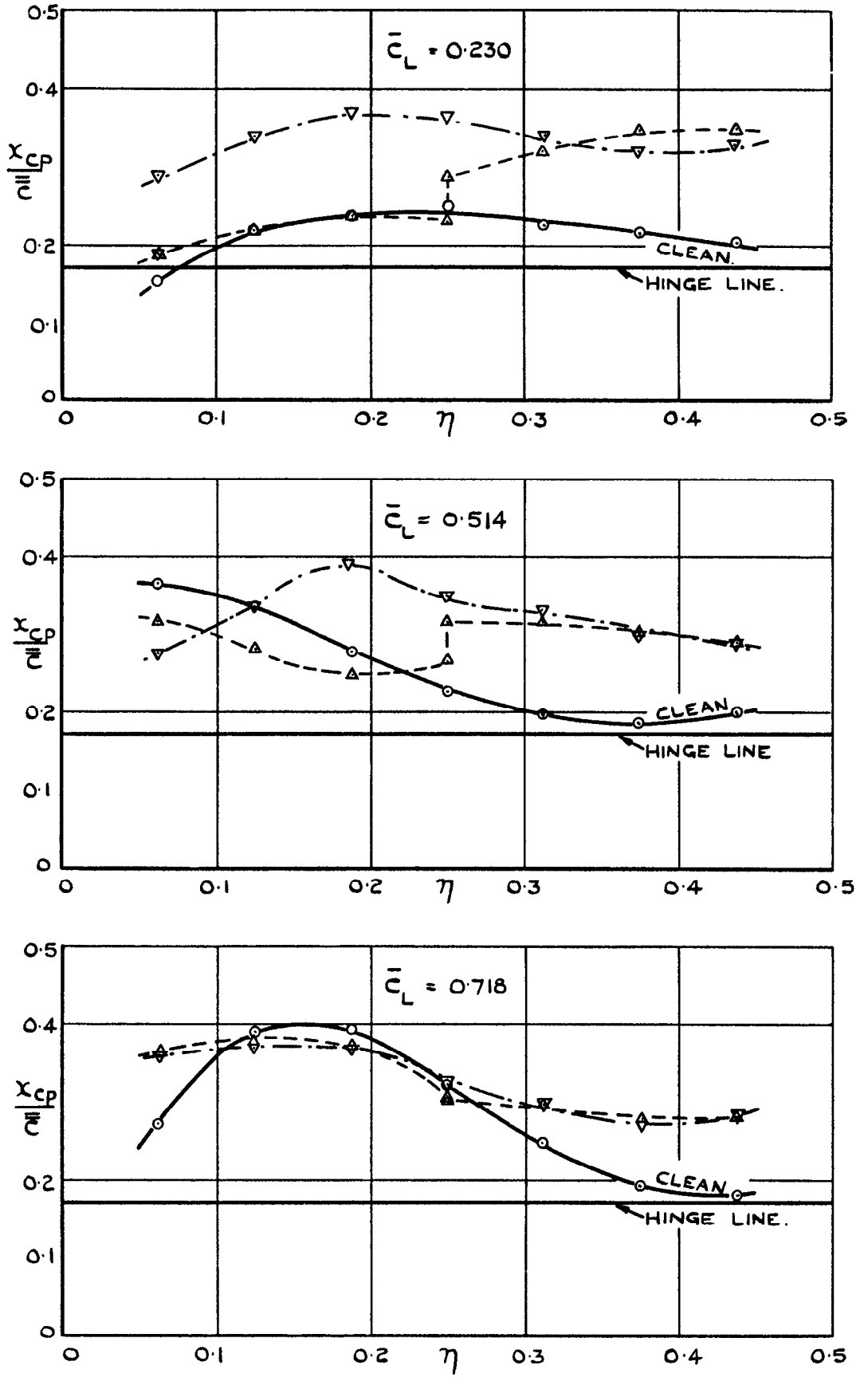

SYMBOLS

CLEAN WING

OUTER NOSEFLAPS DROOPED.

ALL NOSEFLAPS DROOPED.

NOSEFLAP HINGE LINE.

FIG. 26. DISTANCE OF CENTRE OF PRESSURE FROM LEADING EDGE ON INBOARD PANEL OF M-WING.

A.R.C. C.P. No. 577.

533.693.4 :
533.694.2 :
533.69.048.2

LOW-SPEED PRESSURE-PLOTTING TESTS ON A FLAT-PLATE M-WING FITTED WITH PART-SPAN NOSE-FLAPS. Wyatt, L. A. and Ilott, Miss G.P. June, 1960.

Pressure-plotting measurements have been made over the inboard panel of a 55° swept flat-plate M-wing of aspect ratio 5.0 fitted with constant-chord nose-flaps.

The effect of drooped nose-flaps on the pressure distribution over the inboard panel of the M-wing has been found at three overall lift-coefficients of 0.230, 0.514 and 0.718.

Analysis has shown that the loss of stability (pitch-up) which occurs on the M-wing above a lift coefficient of 0.4 can be ascribed to a loss of lift in the neighbourhood of the wing root, and the action of nose-flaps in eliminating this pitch-up has been explained.

A.R.C. C.P. No. 577.

533.693.4 :
533.694.2 :
533.69.048.2

LOW-SPEED PRESSURE-PLOTTING TESTS ON A FLAT-PLATE M-WING FITTED WITH PART-SPAN NOSE-FLAPS. Wyatt, L. A. and Ilott, Miss G.P. June, 1960.

Pressure-plotting measurements have been made over the inboard panel of a 55° swept flat-plate M-wing of aspect ratio 5.0 fitted with constant-chord nose-flaps.

The effect of drooped nose-flaps on the pressure distribution over the inboard panel of the M-wing has been found at three overall lift-coefficients of 0.230, 0.514 and 0.718.

Analysis has shown that the loss of stability (pitch-up) which occurs on the M-wing above a lift coefficient of 0.4 can be ascribed to a loss of lift in the neighbourhood of the wing root, and the action of nose-flaps in eliminating this pitch-up has been explained.

A.R.C. C.P. No. 577.

533.693.4 :
533.694.2 :
533.69.048.2

LOW-SPEED PRESSURE-PLOTTING TESTS ON A FLAT-PLATE M-WING FITTED WITH PART-SPAN NOSE-FLAPS. Wyatt, L. A. and Ilott, Miss G.P. June, 1960.

Pressure-plotting measurements have been made over the inboard panel of a 55° swept flat-plate M-wing of aspect ratio 5.0 fitted with constant-chord nose-flaps.

The effect of drooped nose-flaps on the pressure distribution over the inboard panel of the M-wing has been found at three overall lift-coefficients on 0.230, 0.514 and 0.718.

Analysis has shown that the loss of stability (pitch-up) which occurs on the M-wing above a lift coefficient of 0.4 can be ascribed to a loss of lift in the neighbourhood of the wing root, and the action of nose-flaps in eliminating this pitch-up has been explained.

Published by
HER MAJESTY'S STATIONERY OFFICE

To be purchased from
York House, Kingsway, London w.c.2
423 Oxford Street, London w.1
13A Castle Street, Edinburgh 2
109 St. Mary Street, Cardiff
39 King Street, Manchester 2
50 Fairfax Street, Bristol 1
2 Edmund Street, Birmingham 3
80 Chichester Street, Belfast 1
or through any bookseller

Printed in England

S.O. CODE No.23-9012-77